Structures 51 (2023) 372–390

Contents lists available at ScienceDirect

Structures

journal homepage: www.elsevier.com/locate/structures

Numerical shape, thickness and stacking sequence optimisation and experimental study of hybrid composite plates under in-plane shear loading

Mahdi Damghani [a,*], Jason Matthews [a], Adrian Murphy [b], Carol Featherston [c]

[a] Department of Engineering, Design and Mathematics (EDM), University of the West of England (UWE), Bristol BS16 1QY, UK
[b] School of Mechanical and Aerospace Engineering, Queen's University Belfast (QUB), Belfast BT9 5AG, UK
[c] School of Engineering, Cardiff University, Cardiff CF24 3AA, UK

ARTICLE INFO

Keywords:
Free size optimisation
Hybrid composites
Buckling
Post-buckling
Shear loading

ABSTRACT

Shape, thickness and stacking sequence optimisation of a damage tolerant hybrid (GFRP-CFRP) composite laminate is performed using the commercial Optistruct solver. The results of the optimisation study are compared to both a benchmark non-damage tolerant CFRP laminate (without protective surface GFRP plies known as type 1 laminate) and a damage tolerant traditionally optimised hybrid CFRP-GFRP laminate (having X shape CFRP plies known as type 2 laminate), designed and tested in a previous study. The optimised laminate is manufactured using three different manufacturing techniques. The experimental buckling and post-buckling performance of the manufactured laminates are investigated. The optimised hybrid laminate is approximately 8% heavier than the type 1 but 17% lighter than type 2, but with the benefit of protective surface GFRP plies in favour of a damage tolerant design as shown in a previous study. Both numerical and experimental buckling and post-buckling performance studies show that the optimised laminates demonstrate higher pre-buckling stiffness compared to the type 1 design. However, the experimental buckling and failure/collapse loads, unlike the numerically predicted loads, are 24.31% and 26.70% lower, respectively. This is due to the significant number of ply drop-offs in the hybrid laminate design, and hence geometric imperfections and stress concentration effects at these locations leading to early buckling and failure in the post-buckling region.

1. Introduction

Load bearing composite structures made of Carbon Fibre Reinforced Polymers (CFRP) and Glass Fibre Reinforced Polymers (GFRP) have well-established advantages over their metallic counterparts. Amongst the advantages are higher strength-to-weight and stiffness-to-weight ratios, enhanced fatigue performance, and better corrosion resistance [1]. Additionally, composite materials, due to their laminated nature, have an inherent ability to be tailored to spatially varying design requirements and thus enable large lightweight structures. These properties and design characteristics have been the main drivers for the selection of composites for the manufacture of highly loaded structural components, particularly in aerospace and airframe design [2].

The mechanical performance of composite structures is dependent upon several design variables (fibre angles, ply thickness and material distribution) and manufacturing parameters and constraints. Structural optimisation provides an important tool to manage these variables and constraints. If embedded early in the design process, optimisation enables the creation of designs with minimal mass and maximal stiffness. In recent decades, optimisation methodologies have become an important component in the digital design process of many composite structures, including airframe design [3].

Optimisation of laminated composite stru with the same stacking sequence throughout. Contrastingly, in the variable stiffness scenario, the entire domain is divided into several sub-domains on which different stacking sequences can be materialised. Xu et al. [6] presented a more detailed classification. They considered composite optimisation scenarios in three categories: i) constant stiffness design, ii) variable stiffness design and iii) topology design. The constant stiffness design is analogous to the classification of Ghiasi and Setoodeh [5]. However, in the variable stiffness design, the composite laminate can have a discrete or continuous variable stiffness. In other words, stiffness properties may spatially vary within the component. This stiffness variation may be discrete [7] described by several different patches within a laminate, or continuous [8] varying the fibre angle orientation continuously within a ply's domain. Finally, in a topology optimisation scenario, an optimised

* Corresponding author.
E-mail address: Mahdi.Damghani@uwe.ac.uk (M. Damghani).

https://doi.org/10.1016/j.istruc.2023.03.066
Received 30 January 2023; Accepted 10 March 2023
Available online 20 March 2023

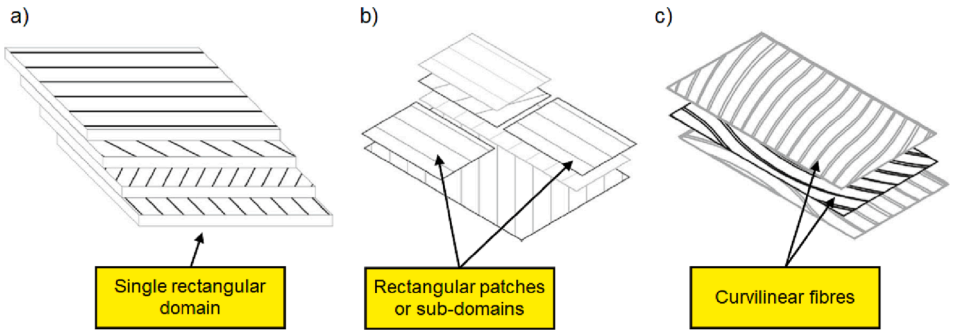

Fig. 1. Illustration of the constant and variable stiffness laminates, a) constant stiffness laminate, b) discrete variable stiffness laminate having rectangular sub-domains and c) continuous variable stiffness laminate with curvilinear fibres [6].

Table 1
Mechanical properties of both woven CFRP (AX-5180) and GFRP (AX 3180) fabric plies [1,23].

Mechanical properties	Units	AX-5180 CFRP	AX-3180 GFRP
$E_{11} = E_{22}$	MPa	67094.00	30083.00
G_{12}	MPa	4831.38	4954.60
S_t*	MPa	595.50	437.16
S_c	MPa	393.00	306.00
S_s	MPa	87.00	62.00
Strain to failure	Strain	0.01	0.02
ϑ_{12} (Poisson's ratio)	N/A	0.04	0.14
t_{ply}^{**}	mm	0.224	0.288

* t, c and s subscripts denote the strength of a ply in tension, compression and shear respectively.
** cured ply thickness.

material distribution may be defined, concentrating the material where it is effective in fulfilling the design constraints is provided [9].

In the literature, optimisation methodologies are categorised as: i) gradient-based methods, ii) heuristic methods and iii) hybrid methods [6]. Gradient-based algorithms are based on the gradient of the objective function and constraints. Although these methods may be computationally expensive, but they have fast convergence. However, they cannot guarantee a global optimum. Heuristic methods do not require gradient information on the objective and constraints, and may find the global optimum using only the values of the objective function and constraints from the previous steps. This is an obvious advantage since in the design of a laminated composite structure the derivative calculations are computationally expensive. Thus, heuristic approaches have been regarded as an effective tool for laminate composite structural design [10]. Heuristic methods include algorithms such as genetic [11], simulated annealing [12], particle swarm [13] and ant colony [14] algorithms. Finally, hybrid optimisation methods combine two or more different optimisation methods. Generally, the purpose of the hybrid method is to produce a global optimum, to obtain a faster convergence or to increase robustness. A popular hybrid approach is to incorporate a gradient-based method into a heuristic method such as a genetic algorithm. From this perspective, the gradient-based local search algorithm is firstly applied to several newly generated design candidates to drive them to local optimal results. Then, the local optimal solutions replace the current candidate designs leading to a higher quality next generation. This strategy amalgamates the advantages of a gradient-based algorithm, i.e. quickly finding an optimal solution, and a genetic algorithm, i.e. achieving the global optimal solution. Hence, the hybrid optimisation methodology needs fewer computations compared to a pure genetic algorithm. The reader is referred to [4,6] for a detailed literature review on optimisation of composite structures.

In the past few decades, despite a considerable body of work on optimisation of laminated composite structures, most work has focused on obtaining either an optimal lay-up for a given loading scenario or

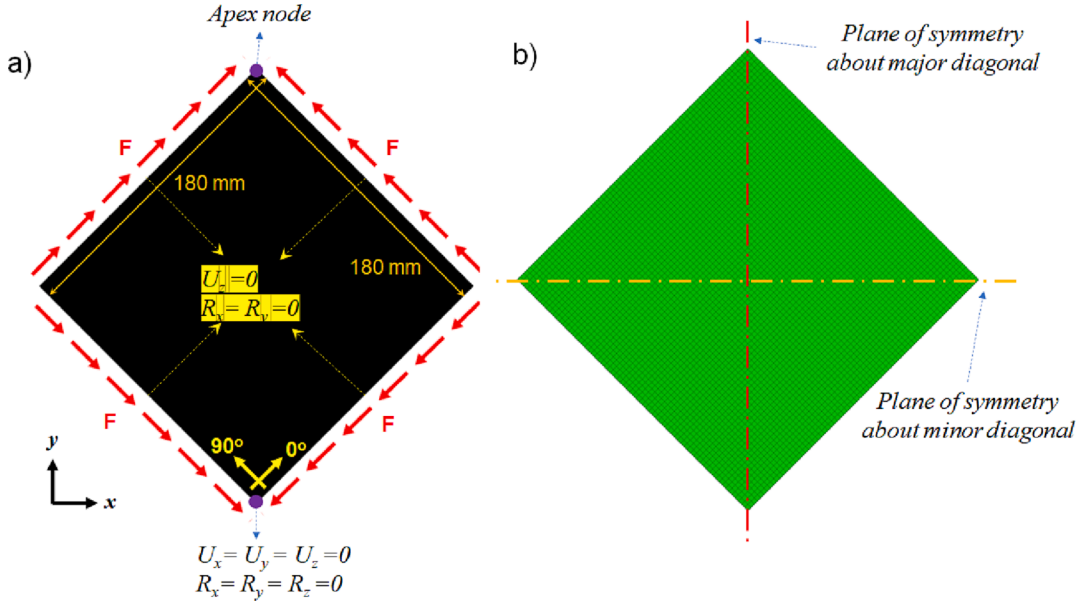

Fig. 2. Structural idealisation of the flat composite laminate panel of study under pure in-plane shear loading, a) loading, boundary conditions and the geometry, b) the mesh density.

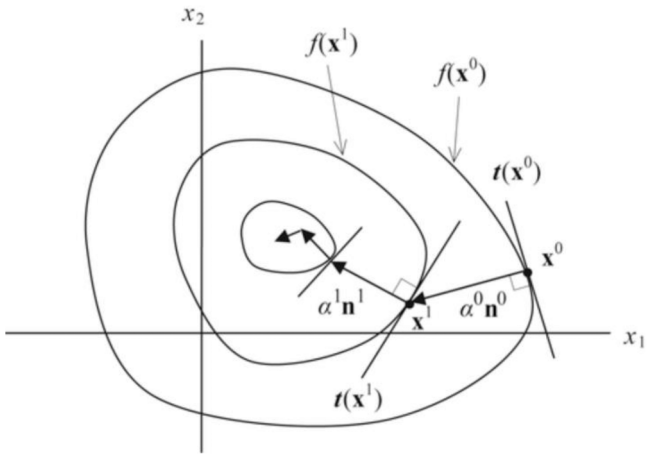

Fig. 3. Schematic illustration of gradient-based approach used in Optistruct [28].

improving the optimisation technology. For instance, Herencia et al. [15] used a hybrid optimisation algorithm to optimise the lay-up of composite stiffened panels. Zhang et al. [16] used a discrete variable stiffness optimisation for cylindrical shells employing numerical finite element analysis to evaluate fitness functions. However, the definition of the shape of the sub-domains was a prerequisite to the optimisation strategy. Bargh et al. [17] carried out the optimisation of symmetrically laminated plates using a particle swarm optimisation algorithm. They used a semi-analytical finite strip method to evaluate the fitness functions. Koide et al. [18] studied a constant stiffness scenario and used an ant colony algorithm to find the optimal stacking sequence of rectangular composite plates under bi-axial compressive loading. Farsadi et al. [19] investigated a variable stiffness optimisation scenario. They used a genetic algorithm to optimise the path of curvilinear fibres considering geometric nonlinearities.

It is evident that these studies are limited to the composite lay-up (both the plies' angle and their stacking sequence) being the dominant design variable with the shape of the composite plies being either fixed or a prerequisite to the optimisation strategy. This is due to the large number of design variables that results when ply shape as well as laminate lay-up are considered together as optimisation variables. Considering ply shape and lay-up together also requires the simultaneous management of continuous and integer design variables. Therefore, such optimisation strategies are often considered infeasible for large structures. Macquart et al. [20] considered both lamination parameters and laminate thickness rather than ply orientations as design variables, to reduce the computational cost of the optimisation. However, they did not include the shape of the plies as a variable. Amongst the few works that did is the work of Bohrer et al. [21]. They proposed a novel strategy employing the method of moving asymptotes and a gradient-based optimiser to simultaneously optimise the topology and stacking sequence of constant stiffness laminates. However, their method assumed that the structure had constant thickness and stiffness limiting the design freedom of their method for wider applications. One of the key difficulties and complexities in shape optimisation of composite laminates is blending [22]. This is to ensure fibre continuity between sub-domains (also referred to as patches) is maintained to ensure a manufacturable structural component. It should be noted that the patches considered in these studies were rectangular in shape further limiting the design space (see Fig. 1).

There is an evident gap in the literature where the optimisation problem includes the shape of the plies, the thickness of the laminate and the stacking sequence as design variables. It is also important to note that the vast majority of studies have only considered a single ply

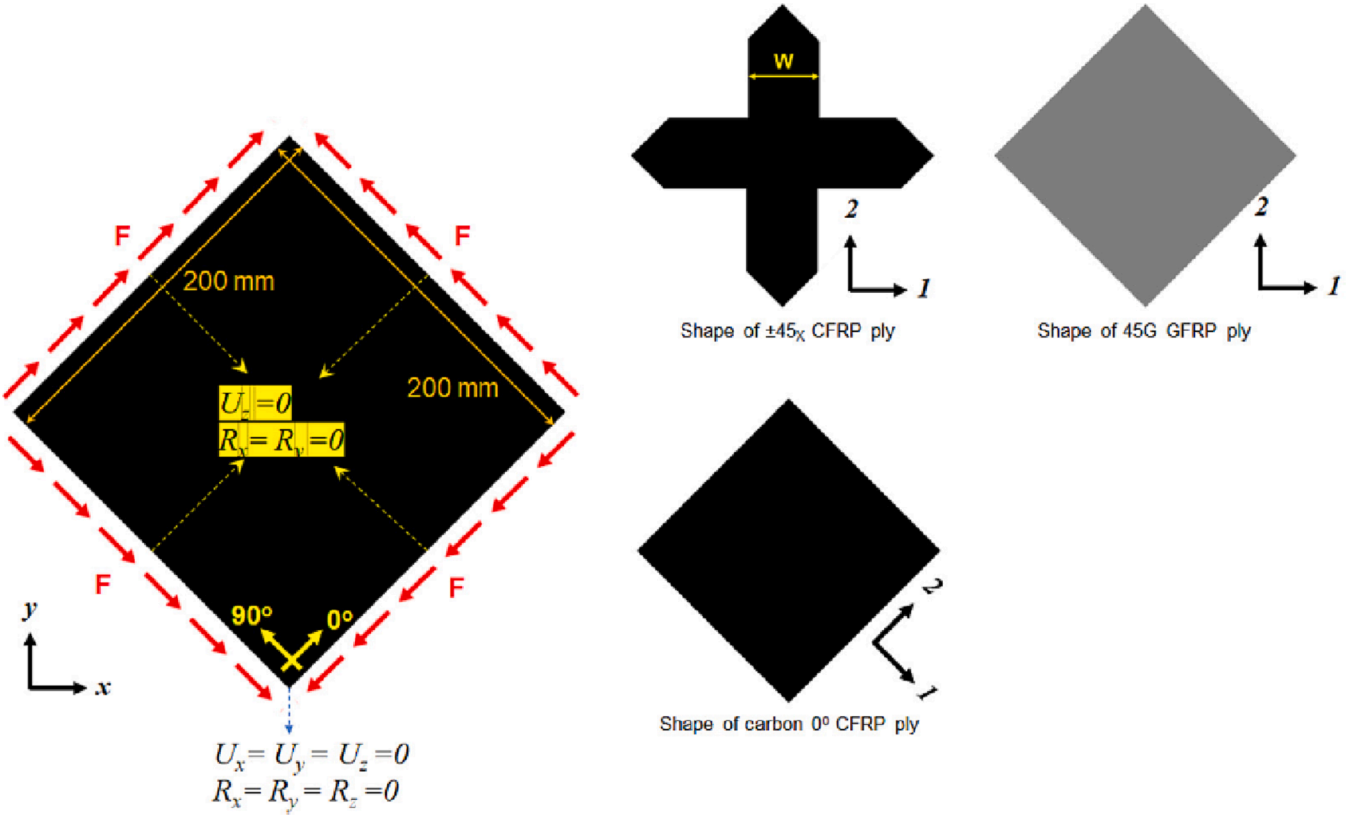

Fig. 4. Structural idealisation of the type 2 flat composite laminate panel studied under pure in-plane shear loading (black plies are CFRP and grey plies are GFRP). Taken from [23,24].

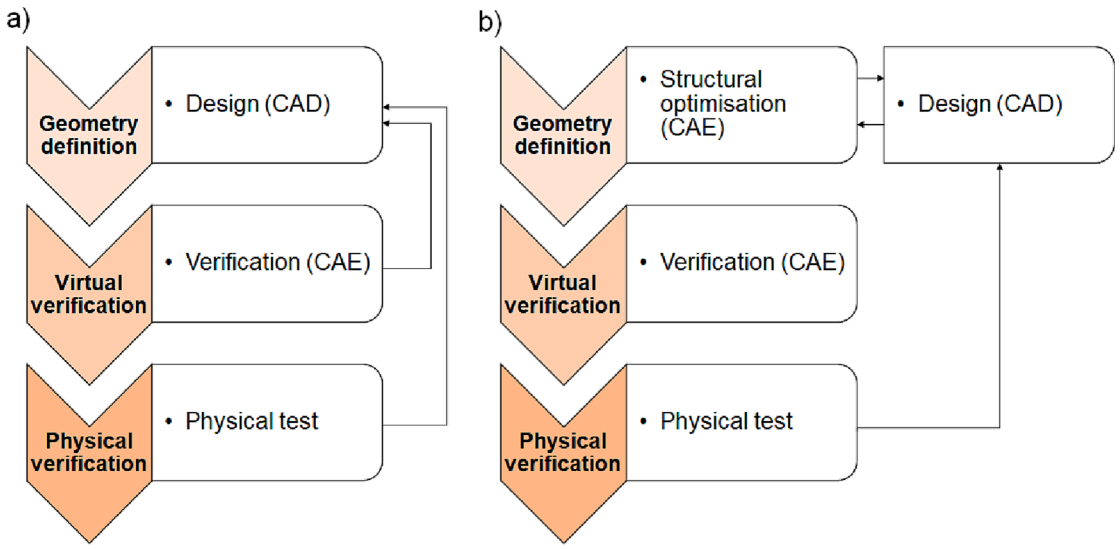

Fig. 5. Flowchart of optimisation and design process, a) traditional design process and b) optimisation driven design process.

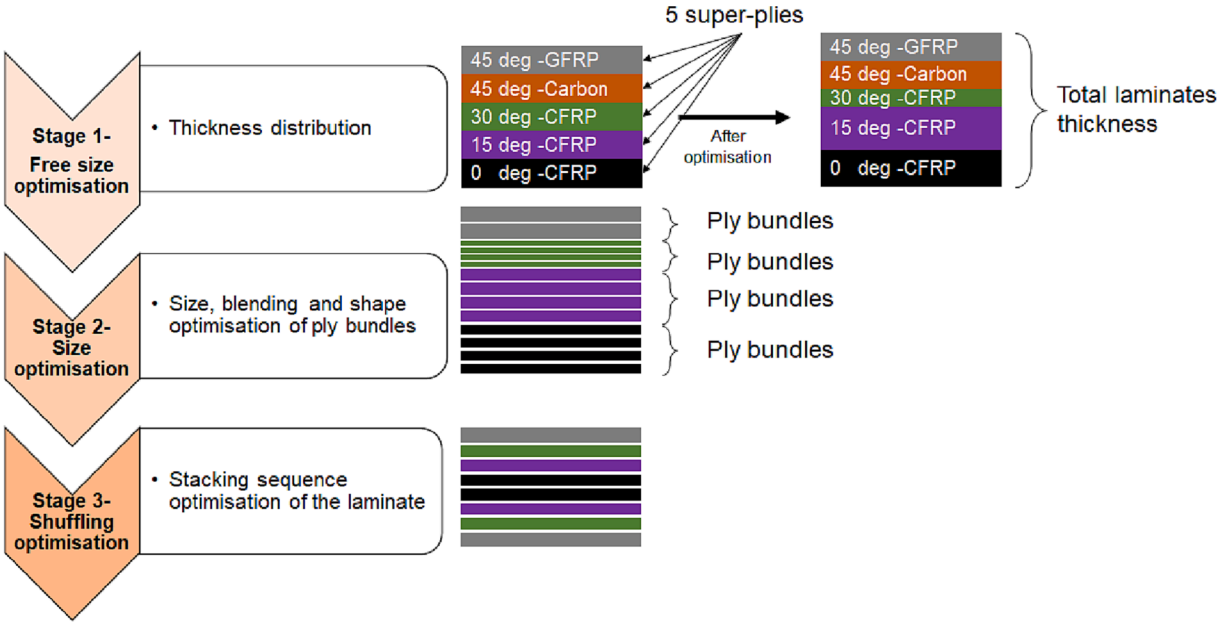

Fig. 6. Composite optimisation process of the current study using optimisation driven design process of Fig. 5b.

material type, either CFRP or GFRP. Considering more than one material does not introduce significant additional problem complexity, only more integer design variables. However, it is more representative of many real-world problems where surface plies are required to fulfil either specific manufacturing or in-service requirements. Furthermore, to the best of the authors' knowledge, experimental validations of the optimised solutions are very much lacking from the literature.

Thus, in this paper, the authors will continue the previous studies [23,24] to optimise a laminated composite plate, representative of an aircraft wing spar web, under pure in-plane shear loading. Simultaneous shape (ply shape), size (laminate thickness) and stacking sequence optimisation (also known as free size optimisation) will be carried out for a woven hybrid CFRP-GFRP laminated composite panel. The optimisation will be executed via a gradient-based optimisation method embedded in the commercial software Optistruct [25]. The optimised panel will be compared with a baseline design initially defined through a traditional parametric simulation study [23]. Three manufacturing techniques will be executed to create the optimised laminate design. Buckling and post-buckling behaviour of the optimised panel will be studied experimentally. Throughout the paper, comparisons will be made with the preceding study by Damghani et al. [23]. Therefore, the novelty of the present work is to bridge the gap in knowledge within the literature: i) to include ply shape design variables along with laminate lay-up variables, ii) to consider a hybrid laminate problem (CFRP-GFRP), and significantly iii) to undertake experimental assessment of the optimised laminate design.

The remainder of this article is organised as follows: in section 2, the overall methodology is presented. This section is divided into four subsections which discuss the key aspects of the proposed method. The materials used in this study are discussed in section 2.1. The finite element modelling technique and laminate optimisation strategy are presented in sections 2.2 and 2.3, respectively. Sections 2.4-2.5 address the manufacturing methods and experimental set up of the study, respectively. Results and discussion are provided in section 3. Finally,

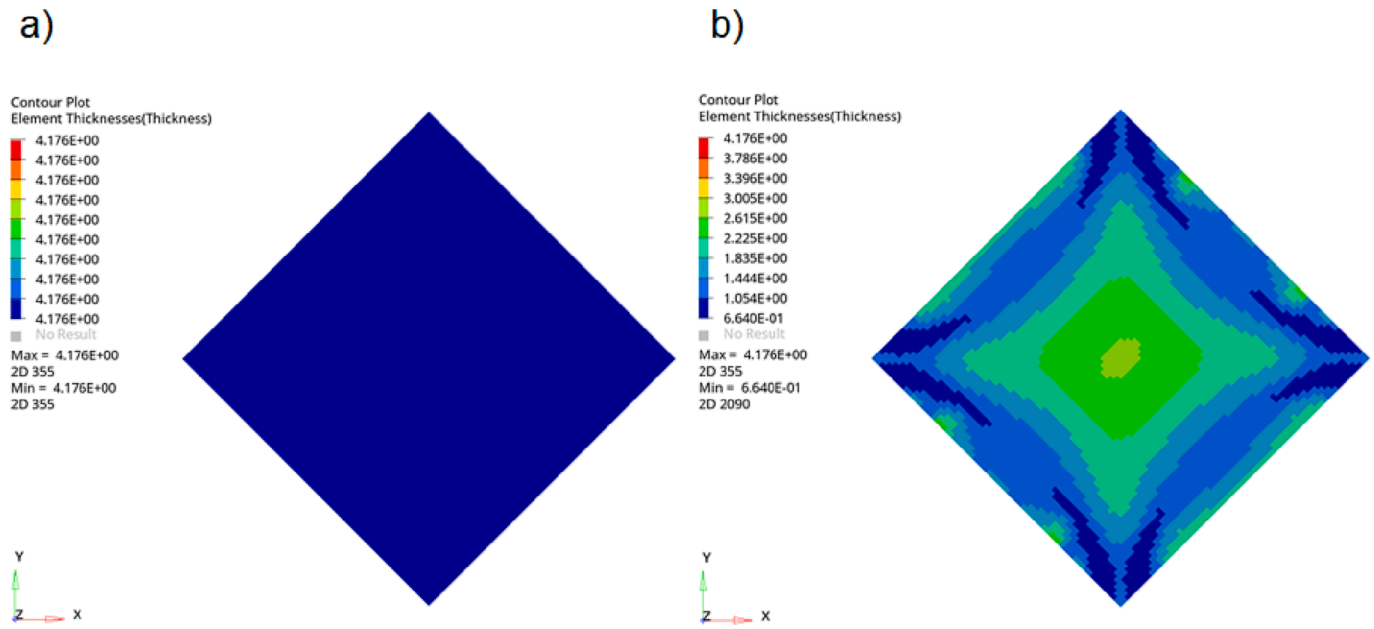

Fig. 7. Evolution of the design (elements' thickness) throughout the optimisation process-stage 1, a) thickness of elements before optimisation, b) thickness of elements after optimisation (all dimensions are in *mm*). For details and shapes of each ply bundle see Fig. 8.

conclusions are made in section 4.

2. Methodology

2.1. Materials

The materials used in this study are twill woven pre-impregnated carbon fibre (AX-5180), and twill woven pre-impregnated glass fibre (AX-3180) with the mechanical properties given in Table 1. Both carbon and glass pre-pregs consist of 54% fibre by volume (60% by weight). These material systems are selected for this study as appropriate data for design has previously been generated and published by the authors [1,23].

2.2. Finite element model (FEM)

In the present study, the commercial Finite Element (FE)-based Optistruct solver [25] is used to perform the analysis and optimisation of the hybrid CFRP-GFRP laminate specimen. A free-size and topology optimisation is undertaken applying the loading, geometry and boundary conditions provided in Fig. 2. For the FEA, the panel loading is idealised as pure in-plane shear loading implemented by application of shell edge loading. This loading idealisation was successfully applied in a previous study validated by experimental results [23]. All edges of the plate are constrained to displace along the z axis. A node at the bottom of the plate is fully clamped with all Degrees Of Freedoms (DOF) constrained. Furthermore, the edges of the plate are suppressed for rotation about both x and y axes (see Fig. 2a) representing the boundary conditions of the experimental test set-up of the study as presented in section 2.5.

A fine mesh density with element size of 2.5*mm* is chosen based on the findings and comprehensive mesh sensitivity studies of [23,24] (see Fig. 2b). Quadrilateral plate elements (CQUAD4) are used to discretise the structure. CQUAD4 elements have 4 nodes and 6 DOFs at each node, i.e. 3 translational and 3 rotational DOFs. CQUAD4 elements utilise 5 integration points as opposed to the standard 4 due to the use of bubble shape functions [26,27], which increase the order of approximation beyond that of a standard linear shell. In other words, bubble functions are interpolating functions that vanish on the element boundary and are higher order than the normal shape functions. Their actual locations and weights are adjusted based on the element configuration. This led to a total of 5184 elements, 5329 nodes and hence 31974 DOFs in the structure.

2.3. Numerical optimisation

In this section, a summary of the optimisation theory and methodology are presented.

2.3.1. Optimisation theory

The optimisation used in this study employs a gradient-based search algorithm. The approach relies on the gradient vector of the objective function ($f(x)$) to determine the search direction in finding an optimal solution. For an objective function of n variables $f(x)$, the gradient vector is defined as [28]

$$\nabla f(\mathbf{x}) = \left[\frac{\partial f}{x_1}\ \frac{\partial f}{x_2}\cdots\frac{\partial f}{x_n}\right]^T$$

The gradient vector at a point x defines the direction of maximum increase in the objective function. Thus, the direction of maximum decrease is opposite to that, i.e. the negative of the gradient vector $-\nabla f(x)$. Any small move in the negative gradient direction will result in the maximum local rate of decrease in the objective function. The negative gradient vector thus represents a direction of steepest descent for the objective function and is written as

$$\mathbf{n} = -\nabla f(\mathbf{x}) = -\left[\frac{\partial f}{x_1}\ \frac{\partial f}{x_2}\cdots\frac{\partial f}{x_n}\right]^T$$

The method of steepest descent, also called the gradient descent method, starts with an initial point $\mathbf{x}^0$ and, as many times as needed, moves from $\mathbf{x}^k$ to $\mathbf{x}^{k+1}$ by minimizing along the vector $\mathbf{n}^k$ extending from $\mathbf{x}^k$ in the direction of $-\nabla f(\mathbf{x}^k)$, the local downhill gradient. The vector $\mathbf{n}^k$, representing the search direction for minimizing the objective function along the steepest descent direction, is normalised as

$$\mathbf{n}^k = \mathbf{n}(\mathbf{x}^k) = -\frac{\nabla f(\mathbf{x}^k)}{\|\nabla f(\mathbf{x}^k)\|}$$

Once the search direction is calculated, a line search is carried out to

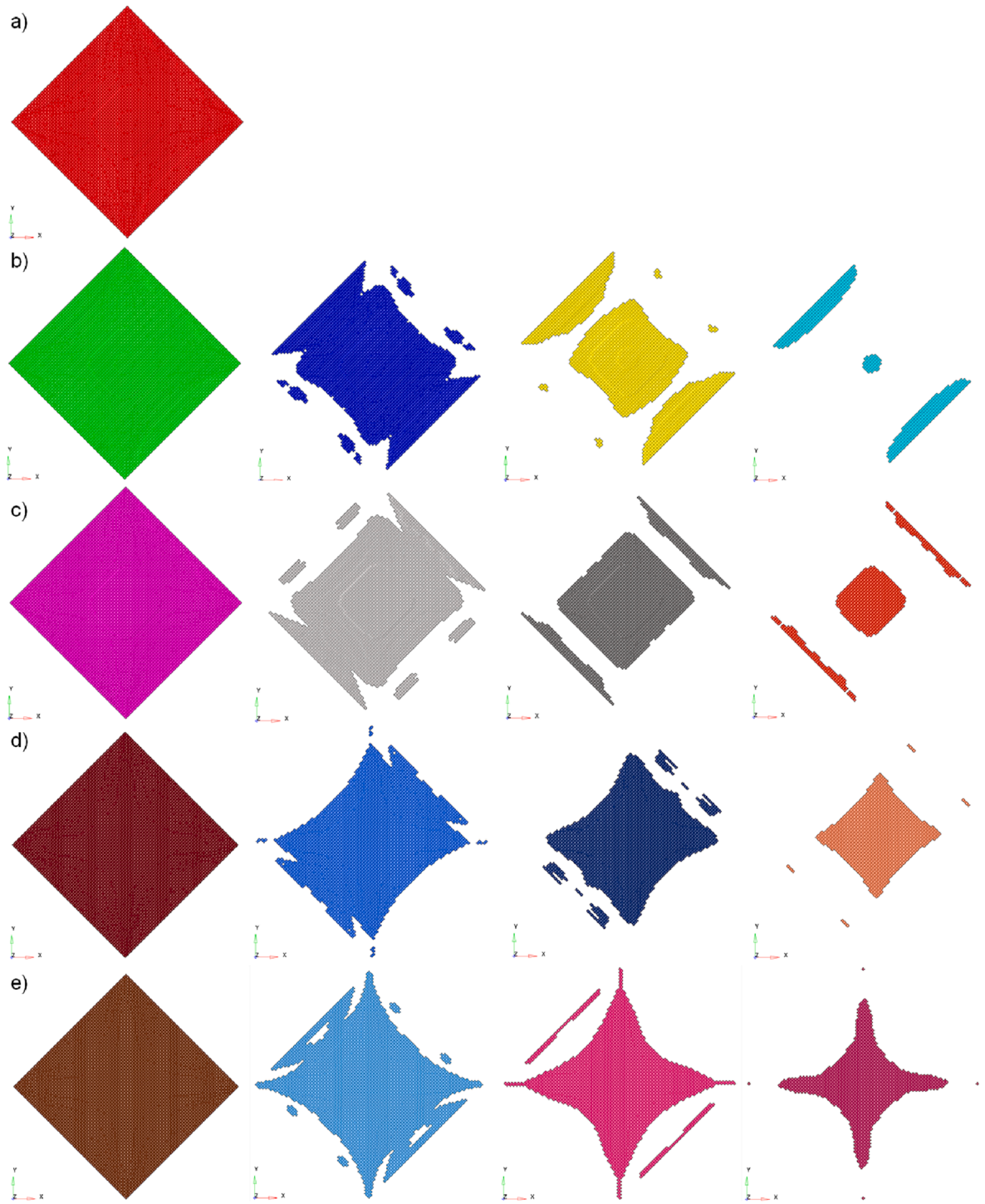

Fig. 8. Ply bundles (4 for each super-ply except for GFRP super-ply) and their shapes for each super-ply of free size optimisation stage for a) 0/90° GFRP, b) 0/90° CFRP, c) 60° CFRP, d) 30° CFRP, e) ±45° CFRP.

find a step size α^k along the search direction. The next design is then determined as

$$\mathbf{x}^{k+1} = \mathbf{x}^k + \alpha^k \mathbf{n}^k$$

This process repeats until the difference in the objective function values of two consecutive iterations is less than a prescribed convergence tolerance ε_1, or the magnitude of the gradient is less than a prescribed tolerance, i.e. $\|\nabla f(\mathbf{x}^k)\| < \varepsilon_2$. Note that geometrically, the steepest descent direction of a design $\mathbf{x}^k$ is perpendicular to the tangent line $t(\mathbf{x}^k)$ of the *iso*-line of the objective function $f(\mathbf{x}^k)$ (see Fig. 3).

2.3.2. Definition of optimisation problem

The experimental performance of the optimised design from this study will be compared with the experimental performance of the laminates reported in [23]. It should be noted that in the previous studies [23,24], two structural configurations were considered. In the first configuration (type 1), the entire laminate was made of woven twill CFRP with a stacking sequence of $[0/0/\pm 45/\pm 45]_S$ and did not possess any damage tolerant design considerations. This was the benchmark laminate in which all CFRP plies had a square shape of $200mm \times 200mm$. The second configuration (type 2) was a hybrid laminate in

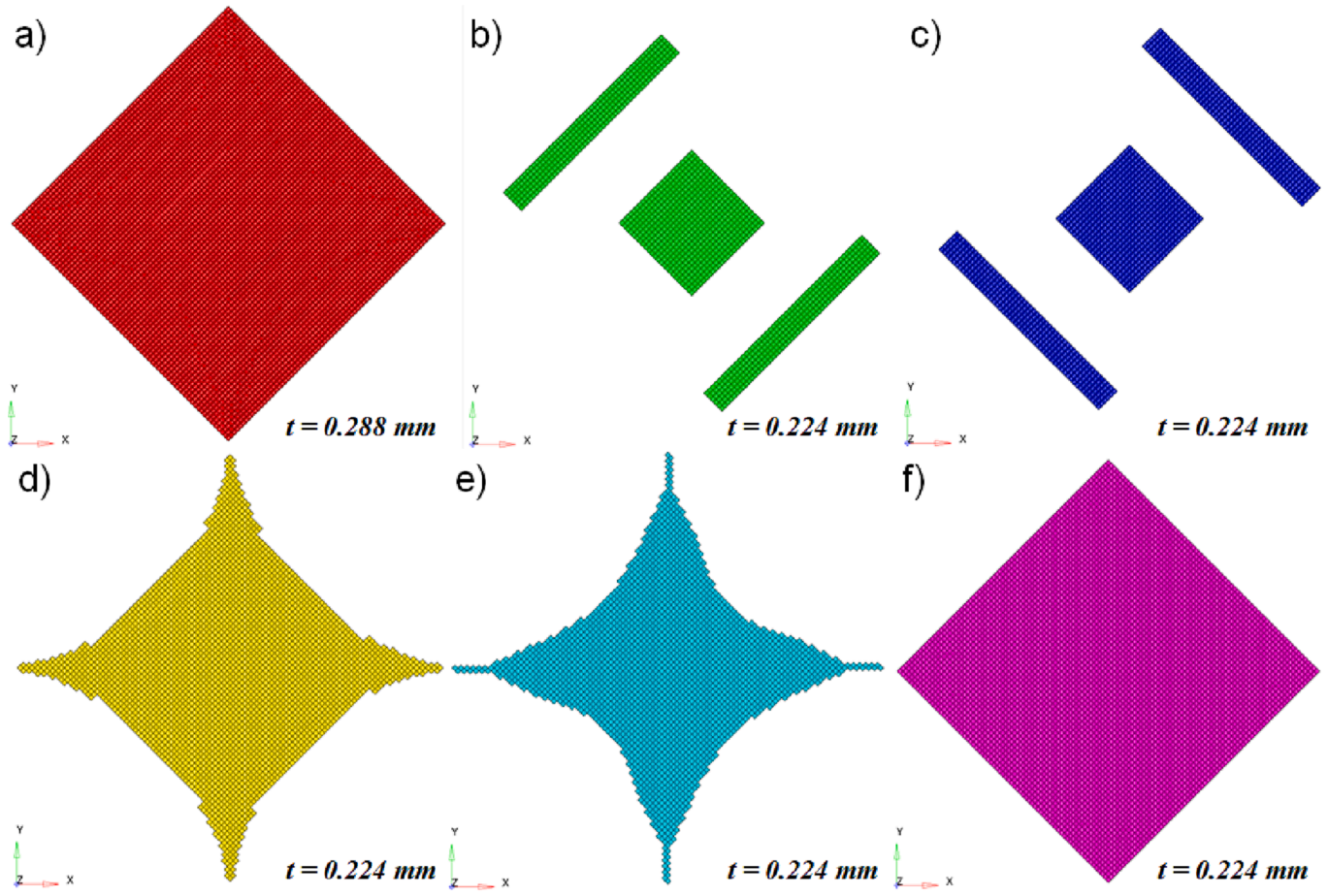

Fig. 9. The shape and orientation of ply bundles and their optimised thickness at the end of size optimisation for a) 0/90° GFRP, b) ±45° CFRP, c) 60° CFRP, d) 0/90° CFRP, e) 0/90° GFRP and f) ±45° CFRP (There are two of above bundles, i.e. 12 in total).

Table 2
Summary of optimisation objective, constraints, and design variables for the current study.

Optimisation stage	Optimisation objective	Design variable	Optimisation constraints
1 2 3	Minimise the mass of the entire laminate	• Thickness of each element • Material orientation of each element • Shape of each ply • Stacking sequence	• Buckling load of the first eigenmode $\geq 32kN$. • Displacement of the apex node A to be $0.45mm \leq \Delta y \leq 0.55mm$. • Symmetry of design about the laminate's diagonals. • Manufacturable ply thickness of 0.224 and 0.288 mm for CFRP and GFRP plies, respectively. • Symmetric and balanced stacking sequence.

which woven twill GFRP plies were placed at the outer and inner mould surfaces. Inclusion of the GFRP plies was to benefit from a damage tolerant design as outlined in [1,29] in detail. It is worth noting that such a damage tolerant design is a necessity and widely used practice in design of wings for aerospace industry. In this hybrid laminate design, both the GFRP and CFRP plies of ±45° angle had a square shape with size $200mm \times 200mm$. However, the CFRP plies at angle 0/90° had an X-shape, as shown in Fig. 4. Thus, the stacking sequence for the type 2 laminate was $[0G/0X/0X/\pm 45/\pm 45]_S$ where G and X represent GFRP and X-shape CFRP plies, respectively. The size of X bracing, i.e. width of X braces (W as in Fig. 4), was obtained using a traditional iterative process as depicted in Fig. 5a.

However, in this study, the authors utilise an optimisation driven design process (see Fig. 5b) using free-size and topology optimisation processes to materialise an optimised composite laminate under in-plane shear loading.

The optimisation problem defined in this study is aimed at identifying the lightest damage tolerant laminate design for a composite structure under pure in-plane shear loading. Such a structure is intended to represent those found in an aircraft wing spar web or even fuselage/wing skin panels where shear loading is significant. The optimised design is examined, and its behaviour is fully studied experimentally. This numerical optimisation is defined as a value function formulated as

Minimise $f(x_1, \cdots, x_n) = M$

where M is the entire mass of the laminate. The design variables, x_i, for the optimisation are the thickness of each element, i.e. 5184 design variables, and the material orientation of each element.

The optimisation is subject to constraints that are defined as

i) The Mode 1 linear buckling load of the laminate is to be equal or higher than $32kN$. This constraint ensures that the buckling load matches that of the type 1 (purely CFRP laminate) of the traditional design study of [23];
ii) A y-direction displacement ($0.45mm \leq \Delta y \leq 0.55mm$) is applied at the apex node A (see Fig. 2) just before the buckling target load ($32kN$ for the mode 1 linear buckling load). This constraint ensures that any optimisation solution will have an in-plane axial membrane stiffness which matches that of the benchmark laminate from [23]).

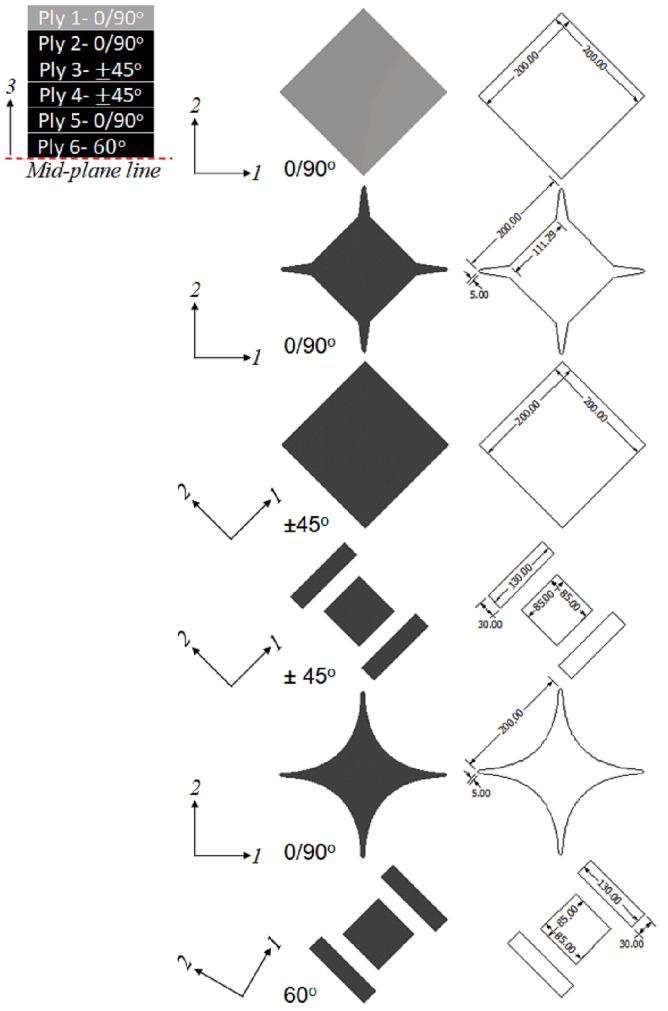

Fig. 10. The shape, orientation, and size of each ply above the mid plane of the optimised laminate at the end of stage 3 (the black and grey plies are CFRP and GFRP, respectively, all dimensions are in *mm*).

iii) Manufacturable constraints are imposed for the entire optimisation process, i.e. ply thicknesses (0.224*mm* for CFRP and 0.288*mm* for GFRP), symmetry of the final lay-up and symmetry of design about the major and minor planes of symmetry as shown in Fig. 2b.

To obtain the above optimisation within the framework of Fig. 5b, the optimisation methodology uses a three-stage process. In stage 1, the concept of super-plies is employed to define a continuous distribution of thickness for each fibre orientation (on an element-by-element basis) that meets the performance requirements of the laminate. By varying the thickness of each ply with a particular fibre orientation for every element, the total laminate thickness can change continuously throughout the structure, thus optimising both the thickness and the percentage of each ply orientation at every point (element). Specifically, within Optistruct, the super-ply functionality enables the thickness of each available fibre orientation to be optimised (to be 'free-sized' in Optistruct terminology). From this perspective, a super-ply is the total designable thickness of a particular fibre orientation. At the design phase, in order to neutralize the effect of ply stacking sequence, the smearing of section properties such as the homogenised Young's modulus and shear modulus are adopted. For this, five super-ply orientations are considered, i.e. 0/90° to ±45° in steps of 15° (see Fig. 6). It is worth mentioning that it is possible to consider smaller step changes in ply orientation such as 2°, 5°, 10°, etc. However, in the current study, the step size of 15° is deliberately used based on existing in-house manufacturing capabilities. Furthermore, since the plies used in this work are woven fabric pre-preg, the ply orientations are in conjugate. For instance, +15° ply represents −75° ply or + 30° ply represents −60° at the same time. This is demonstrated graphically in Fig. 6 and more specifically for the current study in Fig. 7 where the element thicknesses before and after optimisation are provided. It is noteworthy that the lay-up chosen, at this stage, is arbitrary and is not crucial to the optimisation and to the performance of the laminate as the laminate mechanical properties are smeared and homogenised. For stage 1, the thicknesses of each super-ply, i.e. thickness of each element, are considered as the design variables. It should be noted that this constraint has a negligible impact on the optimisation algorithm due to neutralising the stacking sequence effects but does help the optimising algorithm to approach a more reasonable design space.

In stage 2 (see Fig. 6), each super-ply with the thicknesses obtained from the previous stage is split into ply bundles with various shapes as shown in Fig. 8 considering the manufacturable ply thickness. Each bundle represents multiple plies (generally 4 unless specified otherwise as is the case for the GFRP super-ply (see Fig. 8a)) of the same orientation and shape while considering detailed behaviour constraints. It is possible to consider more than 4 ply bundles per super-ply, however experience suggests that the use of 4 ply bundles strikes a good balance between the number of design variables and satisfying the optimisation constraints and objective. Fig. 8b-e shows 4 ply bundles for each super-ply of stage 1. In other words, the ply bundles represent the shape and location of the plies per fibre orientation through element sets. At this stage, the best thickness for each ply bundle is determined. Furthermore, the design is fine-tuned, and ply shapes are tailored for manufacturability as shown in Fig. 9. Since the shapes and thicknesses of some of the ply bundles obtained from Fig. 8 are difficult to manufacture, they are manually adjusted to make them more manufacturable adapting to the available manufacturing process. For instance, some of the generated ply bundles of Fig. 8 have thicknesses less than the manufacturable thickness of 0.224*mm* of the ply. Hence, they are dropped from going to the next stage of the optimisation. As depicted in Fig. 9, during the optimisation, the ply bundles for the 30° CFRP super-ply are dropped and the thicknesses of the other ply bundles are further optimised based on manufacturable thicknesses. It should be noted that the thickness of the GFRP plies is fixed to match that of design type 2 of the previous study [23] as is their position at the outer and inner mould surfaces of the laminate. Thus, they do not participate in the stacking sequence optimisation. In other words, the role of the GFRP plies is to not only provide a protective layer against out of plane impact as demonstrated in [1] but also to increase strain to failure as demonstrated in [23]. Additionally, their stiffness and strength contribution to that of the overall laminate is considered. In summary, at the end of stage 2, 17 ply bundles (see Fig. 8) are reduced to 12 (see Fig. 9). It should be noted that Fig. 9 shows only one out of two of each ply bundle due to symmetry about laminate's mid-plane.

In stage 3, a ply stacking sequence optimisation or otherwise known as shuffling is performed to satisfy all the manufacturing constraints (see Table 2) while delivering optimal performance. Fig. 10 shows the optimised lay-up and the shape of each ply. A summary of the optimisation objective, constraints and design variables for the optimisation process is provided in Table 2.

The numerical eigenmodes and eigenvalues for the final optimised laminate, hereafter known as type 3, and benchmark purely CFRP (type 1) laminate are provided in Fig. 11 and Fig. 12. The optimisation can be seen to have been successful in minimising the mass for a damage tolerant design (incorporating GFRP plies) and yet yielding a 7.63% higher numerical buckling load than type 1.

2.4. Manufacturing method

Due to the complexity of the optimised ply shapes and the number of

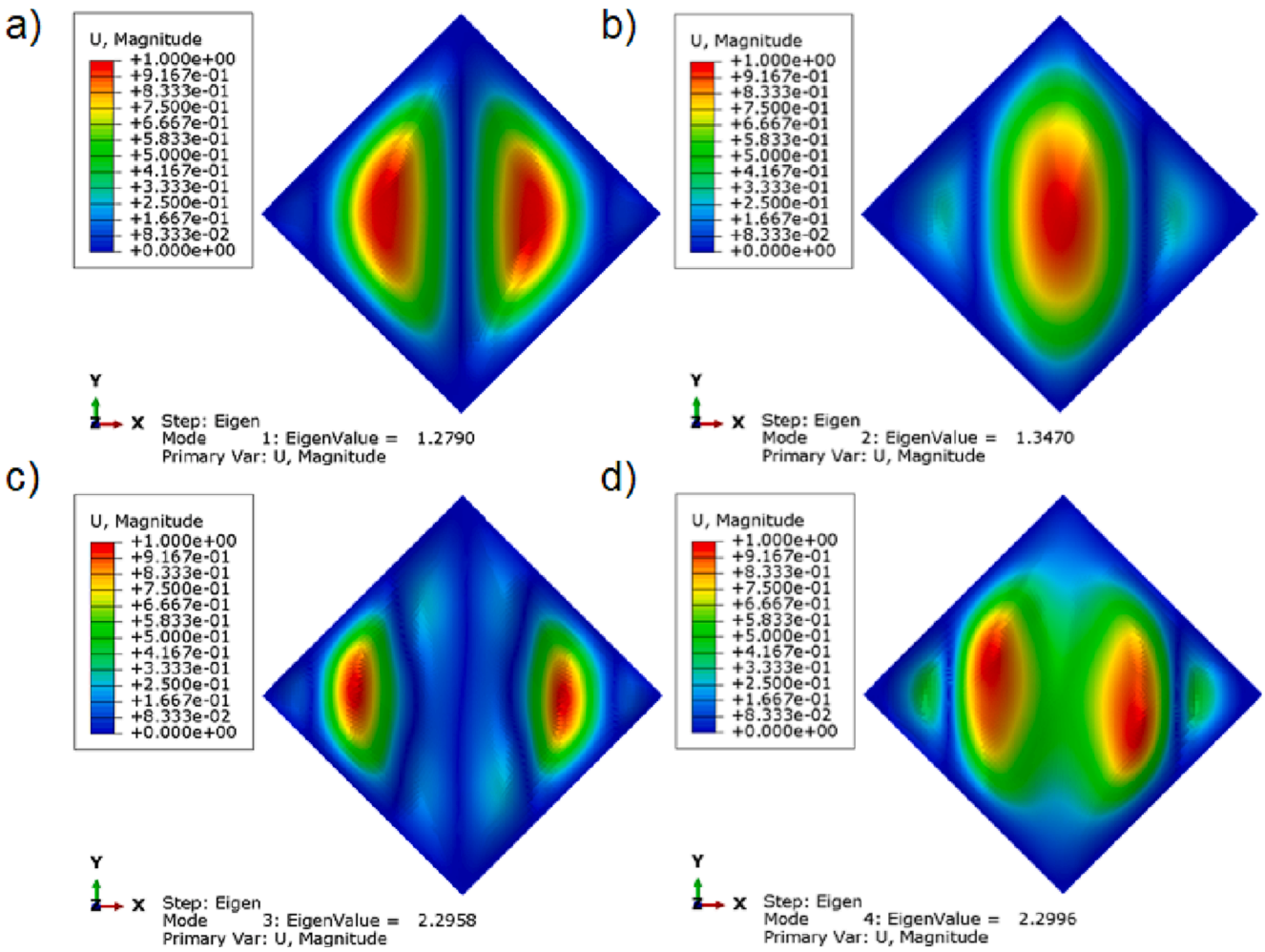

Fig. 11. Numerical mode shapes and buckling load factors (LF) for the first 4 mode shapes of the optimised laminate for applied edge load of $F = 100N/mm$, a) mode shape 1 and LF $= 1.279$, b) mode shape 2 and LF $= 1.347$, c) mode shape 3 and LF $= 2.296$, d) mode shape 4 and LF $= 2.300$.

ply drop-offs, three manufacturing methods are employed to understand the effect of the manufacturing process on specimen performance. Two of the methods are conventional, i.e. hot pressing (HP) and vacuum bagging (VB). The third manufacturing method is an unconventional approach which combines HP and VB to ensure adequate pressure is applied particularly at the ply drop-offs, labelled herein as HP-VB.

In each case, templates are made to the shape of the plies. Then the plies are cut manually to the required shapes shown in Fig. 10. Fig. 13 shows how the manual ply shape cutting and stacking is implemented.

In the HP method, four laminates are initially hand laid up to form a plate and cured in a heated press for an hour at 120° Celsius under 100*psi* pressure. The specimens are then abrasively cut to $200mm \times 200mm$. Similarly, in the VB method, four laminates are hand laid up to form a plate. A vacuum bag is then installed and sealed. A vacuum test is performed to ensure a pressure (14.7*psi*) is applied on the laminates throughout the curing process. The vacuum is applied using an external pump. The vacuum bag is then placed on the press machine, not for pressure but for the heating component of the press machine (see Fig. 14). The heated press is set to 120^oC as of manufacturer's recommendation (AXIOM MATERIALS) and is left for 1 hour. Fig. 15 shows some of the stages of the VB manufacturing process. In the HP-VB process, only a single laminate is made as this was a feasibility study.

2.5. Experimental set-up

The shear test is performed using a 100*kN* capacity INSTRON tensile machine and a picture frame test fixture. The specimens are first clamped into the test fixture via grip plates of width 10*mm*. This leads to gauge dimensions of $180mm \times 180mm$. The specimens are held in position and loaded by constant static friction by the clamping force of the bolts. The specimens and test fixture are positioned in the tensile test machine (see Fig. 16). A tensile load is applied under displacement control at a speed of $2mm/min$. Consequently, this induces a shear deformation to the test laminate.

To acquire strain data, one laminate made using the VB process is instrumented with six uniaxial Vishay strain-gauges (see Fig. 17b) to record strains at a sample rate of 50*Hz*. The locations of the strain gauges are determined based on the laminate eigenvalue simulations, with areas of high strain selected for gauging. Therefore, strain gauges 1 and 3 are positioned at a 40*mm* offset from the centre point of the laminate, i.e. the location of strain gauge 2. To obtain the effect of out-of-plane bending, three extra strain gauges 4, 5 and 6 are located on the back face of the specimens in the same locations as strain gauges 1,2 and 3, respectively. Strain gauges 1, 3, 4 and 6 measure strains in the *x*-direction (Fig. 17), i.e. in the direction perpendicular to the applied tensile loading. Strain gauges 2 and 5 measure strains in the *y*-direction, parallel to the applied tensile loading. Details on the positioning and spacing of each strain gauge and their numbering are given in Fig. 17b.

3. Results and discussions

Fig. 18 shows load–displacement graphs for each of the laminates

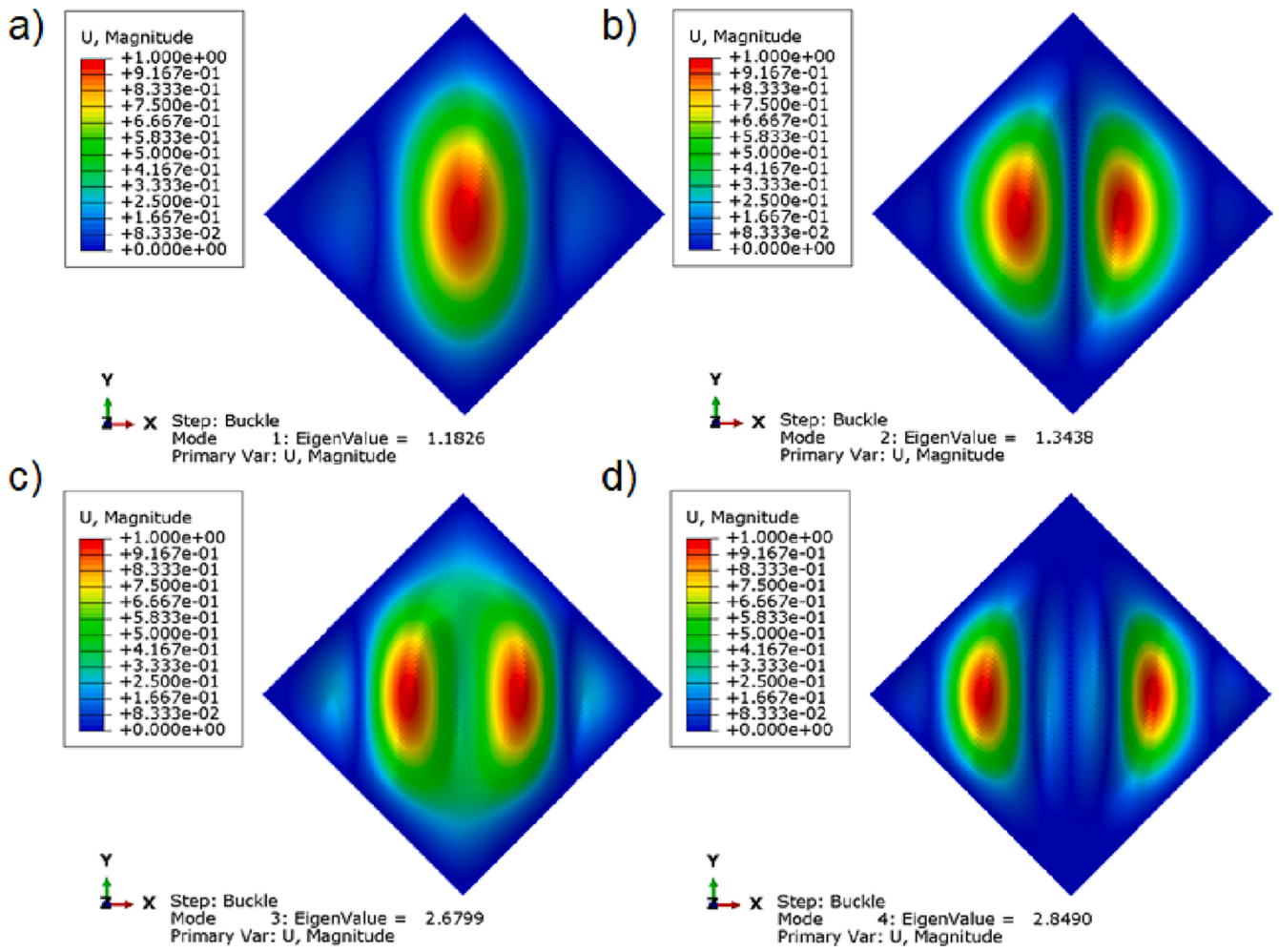

Fig. 12. Numerical mode shapes and buckling load factors (LF) for the first 4 mode shapes of the bench mark purely CFRP laminate (type 1) for applied edge load of $F = 100N/mm$, a) mode shape 1 and LF $= 1.183$, b) mode shape 2 and LF $= 1.344$, c) mode shape 3 and LF $= 2.680$, d) mode shape 4 and LF $= 2.849$.

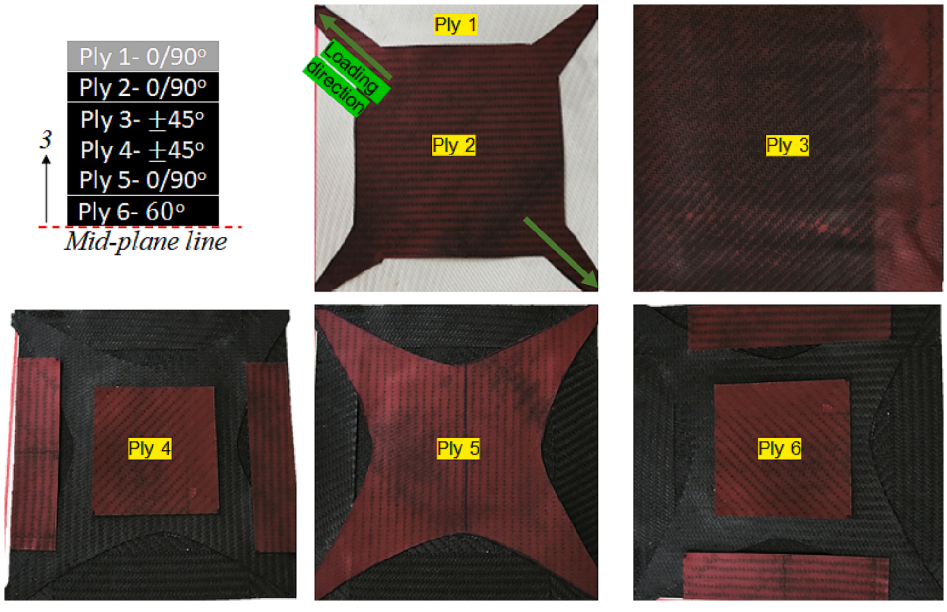

Fig. 13. Overview of the hand lay-up lamination process (shown for half the thickness for a symmetric stacking sequence).

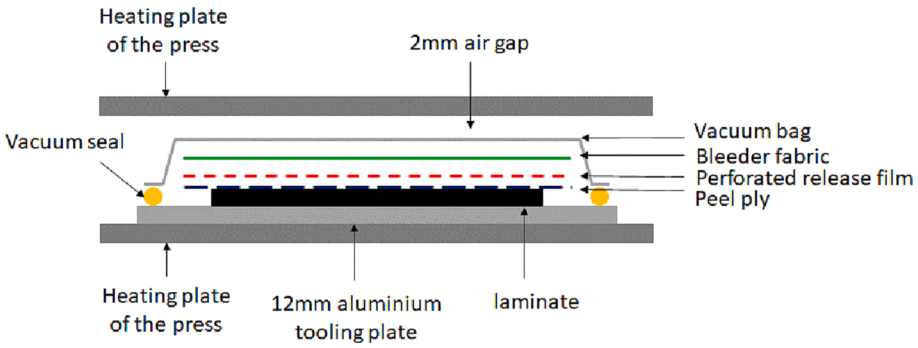

Fig. 14. Schematic of vacuum process for laminates of study.

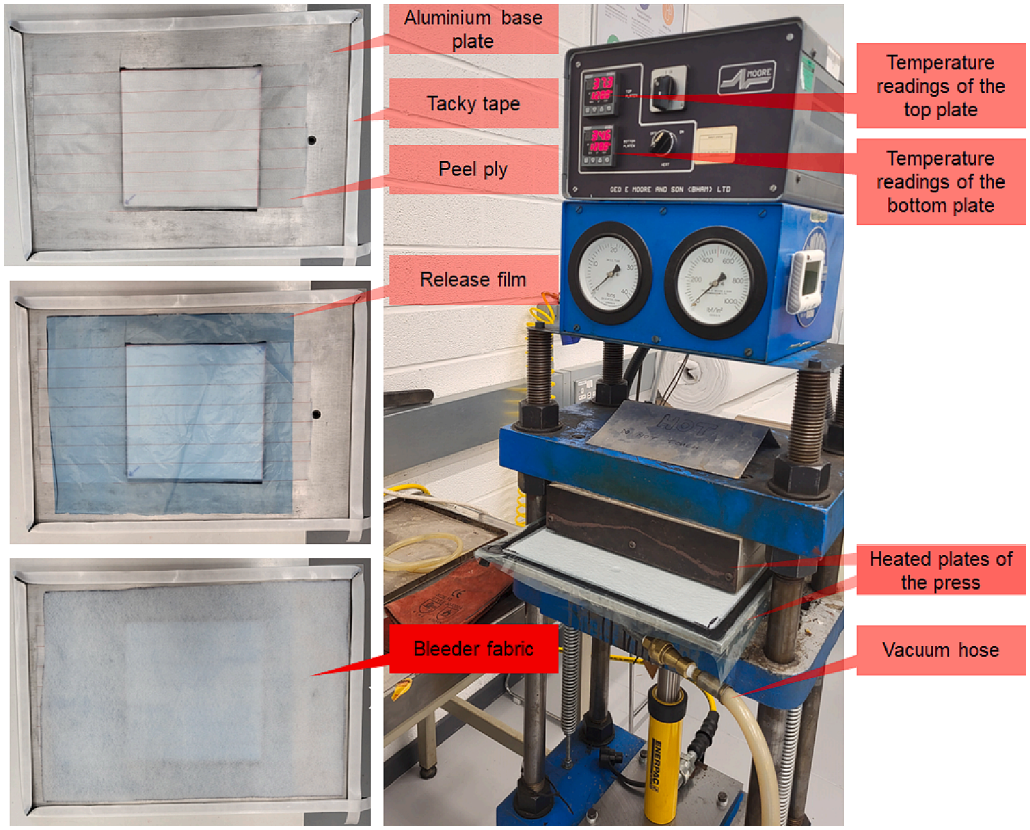

Fig. 15. Overview of the VB manufacturing process.

and includes results from the preceding experiments [23]. Table 3 summarises the preceding laminate designs and introduces specimen labels to enable effective comparison.

The results are also summarised in Table 4. For the sake of clarity, it is worth noting that in the previous study [23], benchmark type 1 laminates were made purely of CFRP plies with no ply shape optimisation and no damage tolerant design considerations. All plies were square in shape and of width and height equal to the specimen's global dimensions, with a stacking sequence of $[0/0/\pm 45/\pm 45]_s$. The type 2 laminates were a hybrid of CFRP-GFRP plies considering a damage tolerant design with 0° CFRP plies having an X shape. In [23], the type 2 laminates had a stacking sequence of $[0G/0_X/0_X/\pm 45/\pm 45]_s$ where G and subscript X represent GFRP plies and X-shape CFRP plies, respectively.

3.1. Performance comparison of manufacturing techniques

Based on Fig. 18, the load–displacement paths from all the tests are characterised by a linear portion until initial buckling (red points in Fig. 18a). The slope of the linear portion i.e. the initial stiffness of the

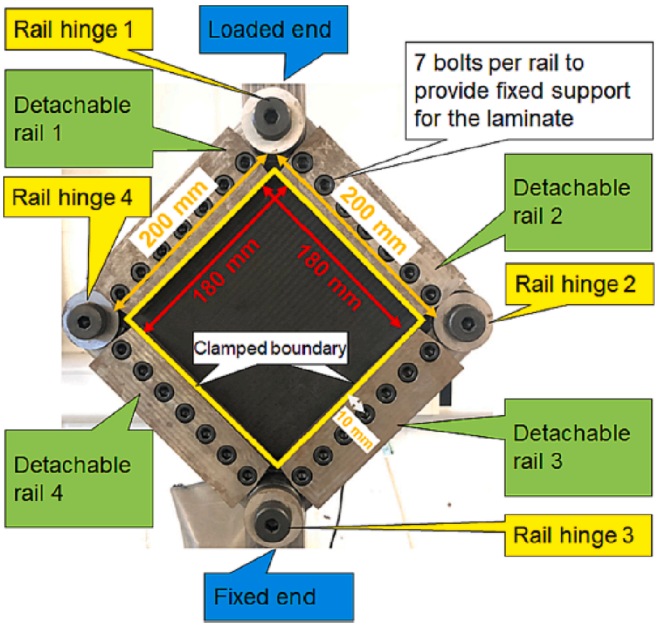

Fig. 16. Schematic representation of in-plane shear test set-up [29].

laminates, is summarised in Table 4. As a result of the out-of-plane displacements at the point of buckling, the stiffness of the laminates drops suddenly after which the load bearing mechanism of the laminates alters as the load is redistributed. After bifurcation, i.e. in the post-buckling regime, the laminates start to behave nonlinearly whilst they endure increasing load. The nonlinear post-buckling behaviour is a result of a combination of geometric and material nonlinearities. The geometric nonlinearities are associated with large out-of-plane displacements whereas the material nonlinearities are the result of matrix cracking and delamination(s) initiated at ply drop-offs (see section 3.3). It is evident that laminates produced by VB were stiffer compared to laminates produced by the HP and HP-VB manufacturing techniques. However, average buckling and failure loads were higher in HP than VB and HP-VB. It is apparent that the HP-VB manufacturing approach has not improved the structural performance beyond that achieved by the HP or VB manufacturing techniques. It should be noted that displacement at failure using VB manufacturing is quite scattered compared to HP. Thus, it could be inferred that, in this study, to achieve laminates of consistent performance, the HP manufacturing approach is preferred to VB. However, HP-VB could provide some advantage in terms of post-buckling strength (considering final failure to initial buckling load ratio).

3.2. Comparison of type 3 to benchmark type 1

Fig. 19 shows the comparison of stiffness, buckling load, failure load and mass of the type 3 laminates (current study) with those of type 1 and type 2 of study [23]. On average, the type 3 laminates showed a 4.24% improved stiffness compared to the benchmark type 1. However, the buckling and failure loads decreased by a significant 24.31% and 26.70%, respectively, compared to type 1. Furthermore, the mass of the type 3 increased by 8.4% relative to the type 1 designs (albeit with a set of protective GFRP plies which are required in many applications to reduce damage resulting from a transverse impact event [1]). However, compared to type 2, type 3 laminate is 17% lighter and 2.6% stiffer but shows 13% and 30% lower buckling and failure loads, respectively.

An experimental reduction of buckling load took place whereas an increase of 7.6% compared to type 1 was predicted by the linear eigenvalue analysis (see Fig. 11 and Fig. 12). The root cause of the reduced experimental buckling and failure loads for the type 3 design could be associated to a significant number of ply drop-offs, not present in the type 1 design. Focusing on ply drop-offs, it is well established in the literature that the resulting material and geometric discontinuity at the ply termination produces a region of high stress concentration [30]. These areas introduce out-of-plane (interlaminar) stresses in addition to in-plane stresses [31]. Thus, these areas are likely locations for fibre fracture, matrix cracking and more predominantly delamination [32].

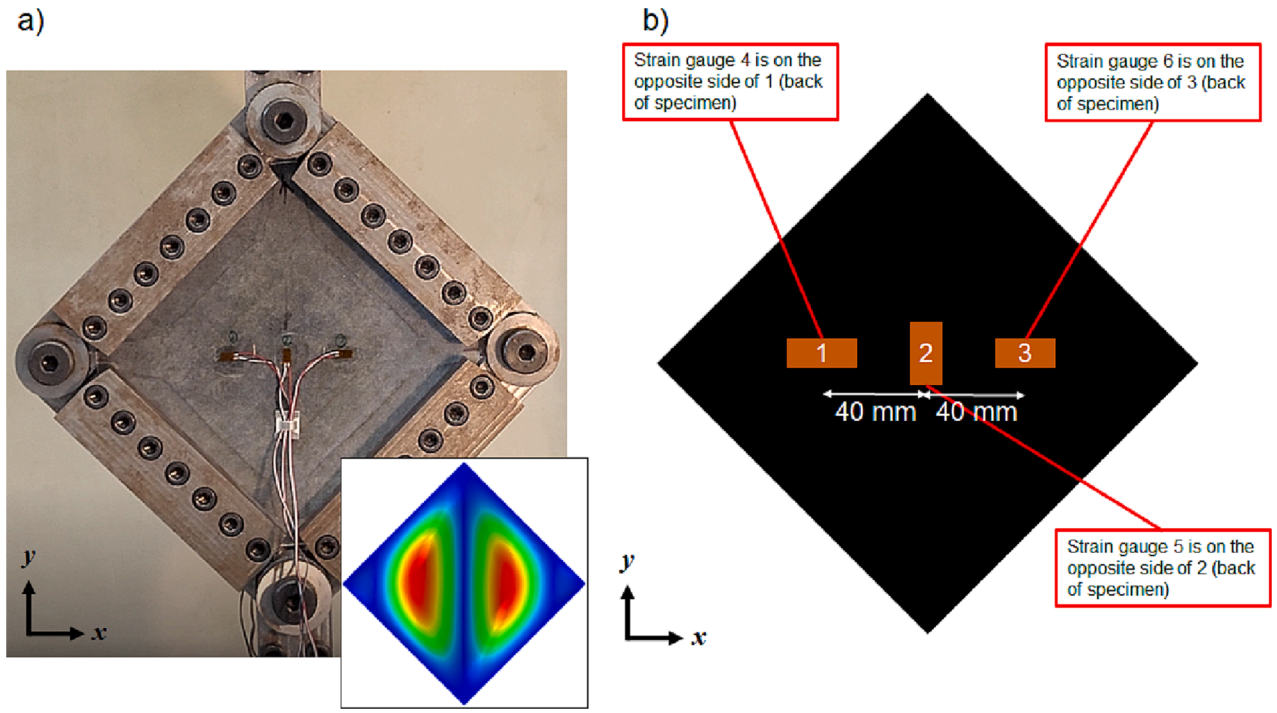

Fig. 17. Shear test set-up; a) gauged laminate and b) location of strain gauges and their numbering (strain gauges 4, 5 and 6 are on the back of the laminate opposite to strain gauges 1, 2 and 3, respectively. The contour plot shows first numerical mode shape of the laminate).

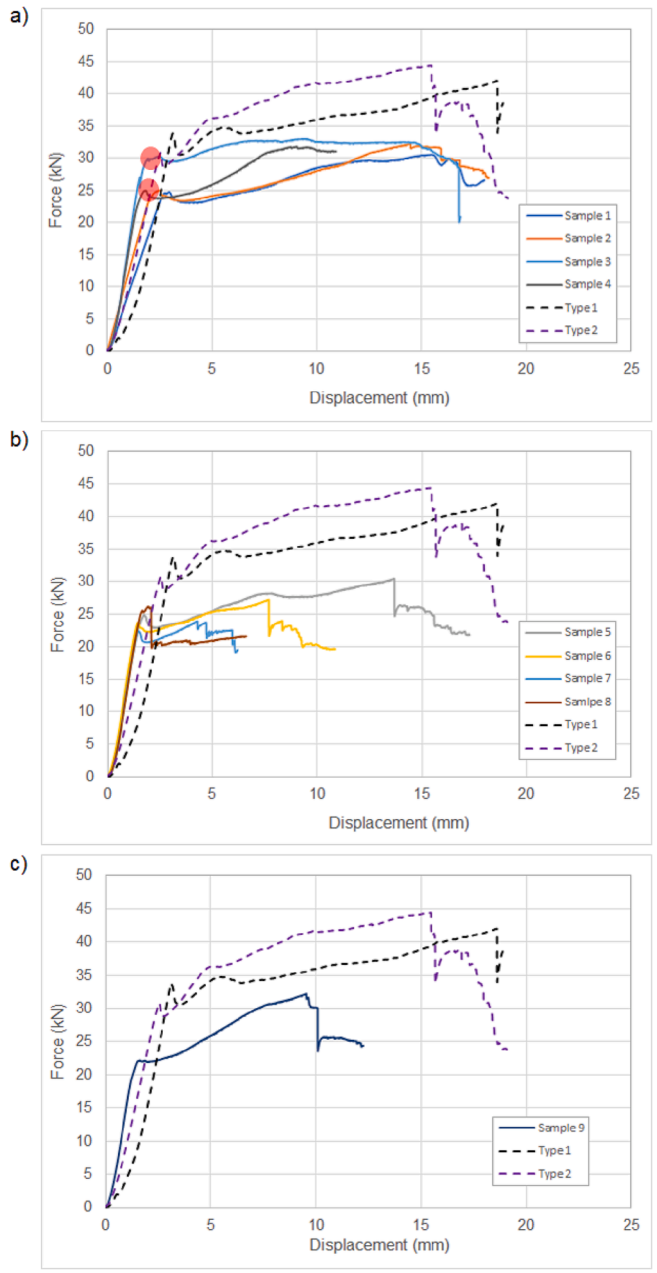

Fig. 18. Load-displacement graphs for laminates made by a) HP, b) VB and c) HP-VB manufacturing methods compared with those of type 1 and type 2 laminates from study [23] (dashed lines).

Hence, this could lead to early failure of the components before the ultimate load carrying capacity of the laminate is reached. Additionally, ply drop-offs, in this study, are the sources of load eccentricities at the pre-buckling phase that lead to secondary bending moments within the laminate (see Fig. 20). In other words, they perform as initial imperfections in the form of out-of-plane bending moments (about axis *y* of Fig. 20), potentially accelerating the buckling of laminates. Additionally, based on Torres et al. [33] ply drop-offs are singular details in composite structures and require methods such as the Multi-Instrumented Technological Evaluator (MITE) approach to study their mechanical performance. In this study, consideration of failure at the ply drop-offs in the post buckling region would require a three-dimensional (3D) local FEM with high fidelity. This would have made the optimisation routine very computationally expensive and therefore impractical considering that ply shapes and hence the ply drop-offs locations continuously change throughout the optimisation process. It should be noted that to date there is no commercial or non-commercial tool to consider such complexities for composite optimisation process. Thus, consideration of such detail complexities is identified as a clear gap in knowledge and the use of existing tools such as Optistruct should be implemented bearing these difficulties in mind. Future work will consider how an additional design stage could be added to the proposed process (see Fig. 6), to account for strength reduction resulting from ply drop-offs.

3.3. Damage mechanisms

Figs. 21–23 show the damage mechanisms for HP, VB and HP-VB manufacturing techniques using visual inspection, respectively, at different points along the load–displacement path. In all manufacturing methods, there is no damage up to the point of buckling. This observation suggests that, in this study, all manufacturing techniques are suitable up to the point of buckling. Immediately after buckling, matrix cracking was present. After buckling up to the point of failure/collapse load, matrix cracking was the only dominant failure form. However, at the failure load, fibre fracture was dominant for the HP and HP-VB samples whereas delamination was the main failure mode for the VB samples. It is worth noting that, for all manufacturing methods, the damages were initiated at ply drop off locations particularly at those of 60° plies (ply 6) where stress concentrations are deemed to be high.

3.4. Experimental buckling mode shape

Fig. 24 shows the buckling mode shape and strain gauge readings 1-6. As shown, the experimental buckling mode shape is unsymmetric about the main diagonal (yellow dashed line). The mode shape is similar to the numerical mode 1 but more biased to the left, which equates with the higher compressive strain readings of strain gauge 1 relative to strain gauge 3. In other words, the buckling mode shape can be approximated as a linear superposition of numerical modes 1, 2 and 3, see Fig. 11. Furthermore, deviation of the readings of strain gauge 1 from those of strain gauge 4 shows the occurrence of bending after buckling pivoting about the main diagonal. Additionally, strain gauges 2 and 5 show tensile strains in the direction of the specimens' main diagonal. The discrepancies in the readings of these two strain gauges suggests slight out-of-plane bending pivoting about the minor diagonal (orange dashed line). It is worth noting that the manual nature of cutting the plies and inherent lack of full precision in doing so could have contributed to the unsymmetric buckling mode shape in the experiment. Additionally, the presence of the ply drop-offs and variation in their location could have resulted in geometric imperfections resulting from manufacture which could have negative influence on the initial buckling load.

4. Conclusions

Numerical shape, thickness and stacking sequence optimisation of a damage tolerant composite hybrid (GFRP-CFRP) laminate square plate was undertaken. The plate design was optimised considering in-plane

Table 3
Summary of specimens.

Study	Process	Label used in graphs		Material	Design
Current study	HP	Type 3	Sample 1	CFRP-GFRP**	0/90, ±45, ±60 CFRP ply shaping
			Sample 2		
			Sample 3		
			Sample 4		
	VB		Sample 5		
			Sample 6		
			Sample 7		
			Sample 8		
	HP-VB		Sample 9		
Preceding study [23]	HP	Type 1		CFRP***	No ply shape optimisation with stacking sequence $[0/0/\pm 45/\pm 45]_s$
	HP	Type 2		CFRP-GFRP**	CFRP ply shaping with stacking sequence $[0G/0_X/0_X/\pm 45/\pm 45]_s$*

* where G and subscript X represented GFRP plies and X-shape CFRP plies, respectively.
** damage tolerant design.
*** non-damage tolerant design.

Table 4
Summary of average of stiffness, buckling load and failure load of type 3 (optimised laminate) for various manufacturing methods.

Manufacturing method	Design type	Number of samples	Stiffness (kN/mm)	Buckling load (kN)	Failure load (kN)
HP	3 ***	4	12.009 ± 1.96 *	26.250 ± 2.514	32.462 ± 1.332
VB		4	15.398 ± 0.416	24.390 ± 1.690	26.964 ± 2.726
HP-VB		1	14.827	22.027	32.234
Total average **		9	14.078 ± 1.189	24.222 ± 2.102	30.553 ± 2.029
HP	1 ****	1	13.505	32.000	41.680
HP	2 ****	2	13.712	27.900	43.940

* ± shows standard deviation.
** Average over all manufacturing types, i.e. 9 laminates.
*** Free size optimisation of current study.
**** Taken from study [23].

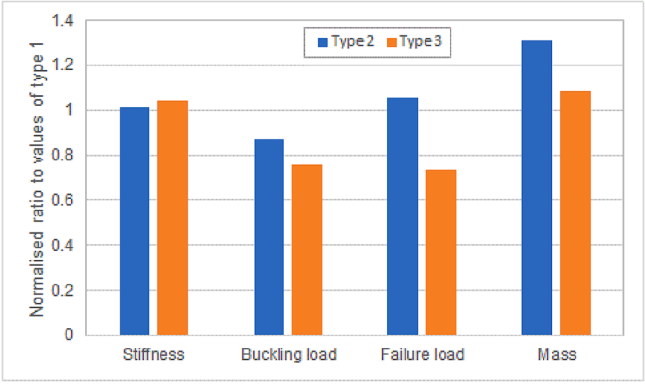

Fig. 19. Stiffness, buckling and failure loads and mass comparison of type 3 (free-size optimised laminates of study) and type 2 (traditional optimisation of damage tolerant laminate [23]) with type 1 of study [23]. All values are normalised to those of benchmark type 1 laminates.

shear loading with the commercial Optistruct solver used to perform a gradient based optimisation. The results of the optimisation study were compared to a benchmark CFRP laminate which had ply dimensions constrained to the plate specimen geometry, i.e. without ply shape optimisation. The optimised laminate was manufactured using three different manufacturing techniques - hot pressing (HP), vacuum bagging (VP), and a process combining hot pressing and vacuum bagging (HP-VP). The buckling and post-buckling performance of the manufactured laminates were studied experimentally. It was shown that the hybrid laminate was ≈ 8% heavier than the benchmark which was without protective GFRP plies, i.e. non-damage tolerant design. For all manufacturing techniques, the hybrid specimens had no failure up to the buckling load, after which matrix cracking was present throughout the post-buckling regime until the failure load. At failure, fibre fracture was present for the HP and HP-VB specimens, whereas delamination was dominant for the VB specimens. The buckling and post-buckling performance studies showed that the hybrid damage tolerant laminates demonstrated higher stiffness compared to the benchmark design (without the protective GFRP plies). However, the experimental buckling and failure loads were 24.31% and 26.70% lower, respectively. In comparison, the linear analysis used for the design optimisation predicted a higher buckling load than that achieved by the benchmark design. The reason for these discrepancies is assumed to be the existence of geometric imperfections induced by significant number of ply drop-offs influencing the initial buckling load and their failure in the post-buckling region, impacting the maximum load the specimen could carry. The major conclusion from this work is that shape, thickness and stacking sequence optimisation may be used to offset the mass of protective GFRP plies in a damage tolerant hybrid laminate only if the failure mechanisms introduced by hybridisation and ply shaping are fully represented in the optimisation analysis and minimised by careful consideration of manufacturing methods. Otherwise disparity between the existing commercial and non-commercial numerical optimisation methods and experimental results will be inevitable and the numerical results should be inferred by caution.

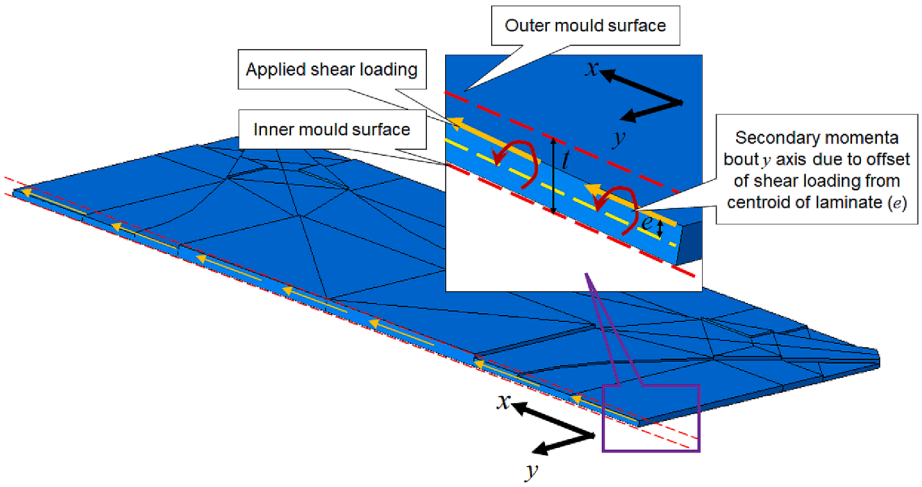

Fig. 20. Illustration of secondary induced bending moments due to ply drop offs. (Red moments are induced due to eccentricity of applied orange shear load with local centroid (yellow dashed lines) at drop off locations). (For interpretation of the references to colour in this figure legend, the reader is referred to the web version of this article.)

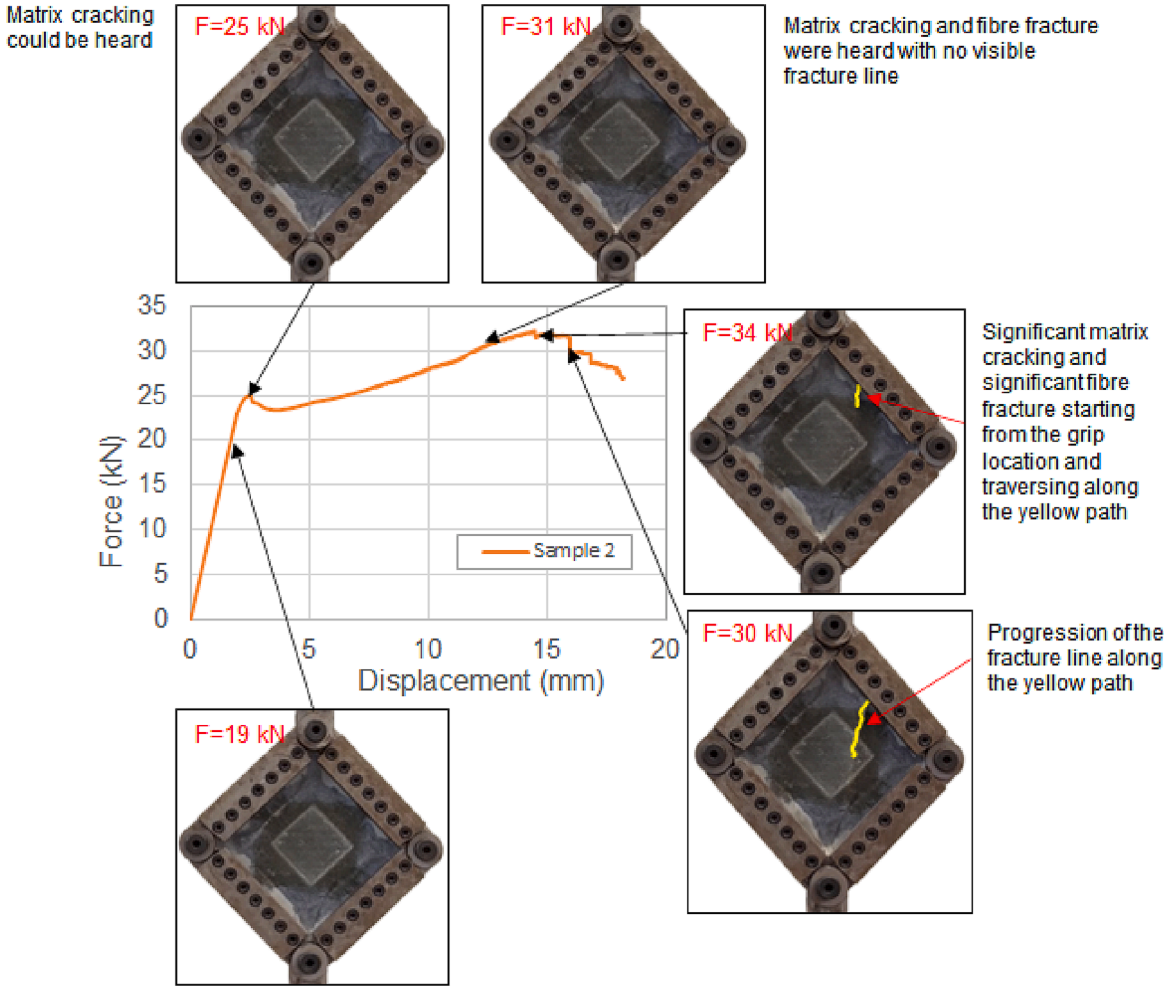

Fig. 21. Progression of damage in sample 2 produced by the HP technique.

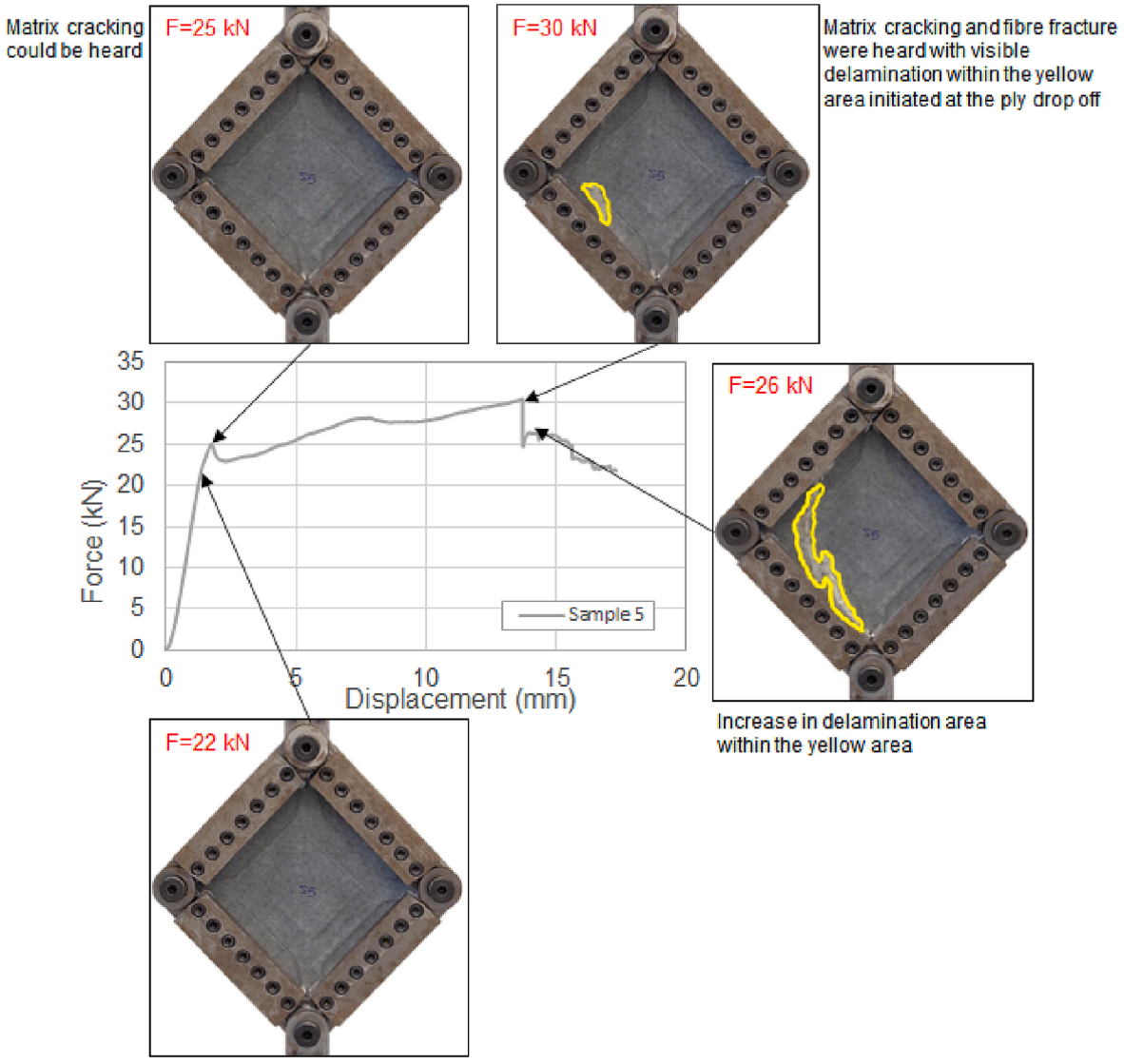

Fig. 22. Progression of damage in sample 5 produced by the VB technique.

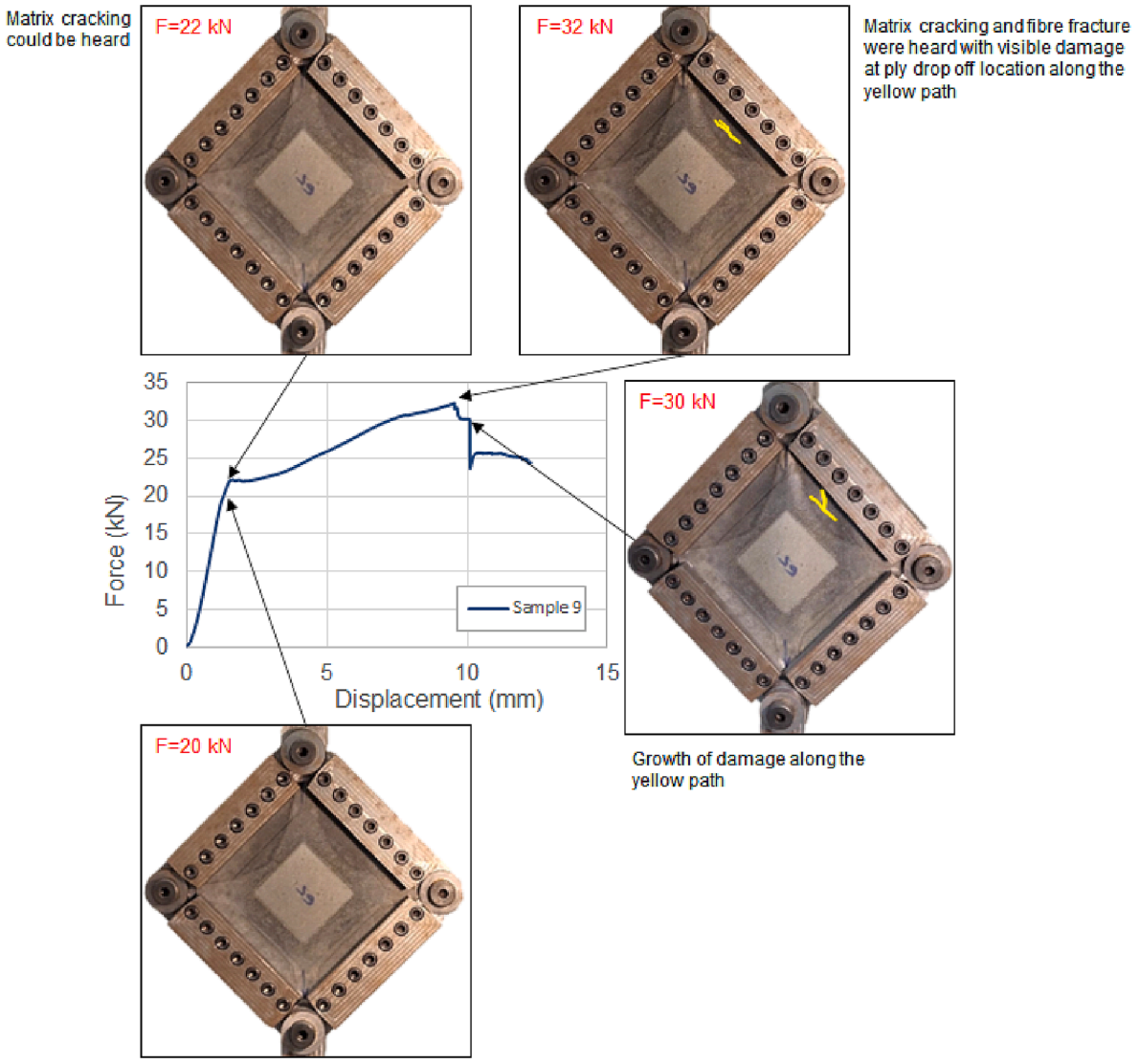

Fig. 23. Progression of damage in sample 9 produced by the HP-VB technique.

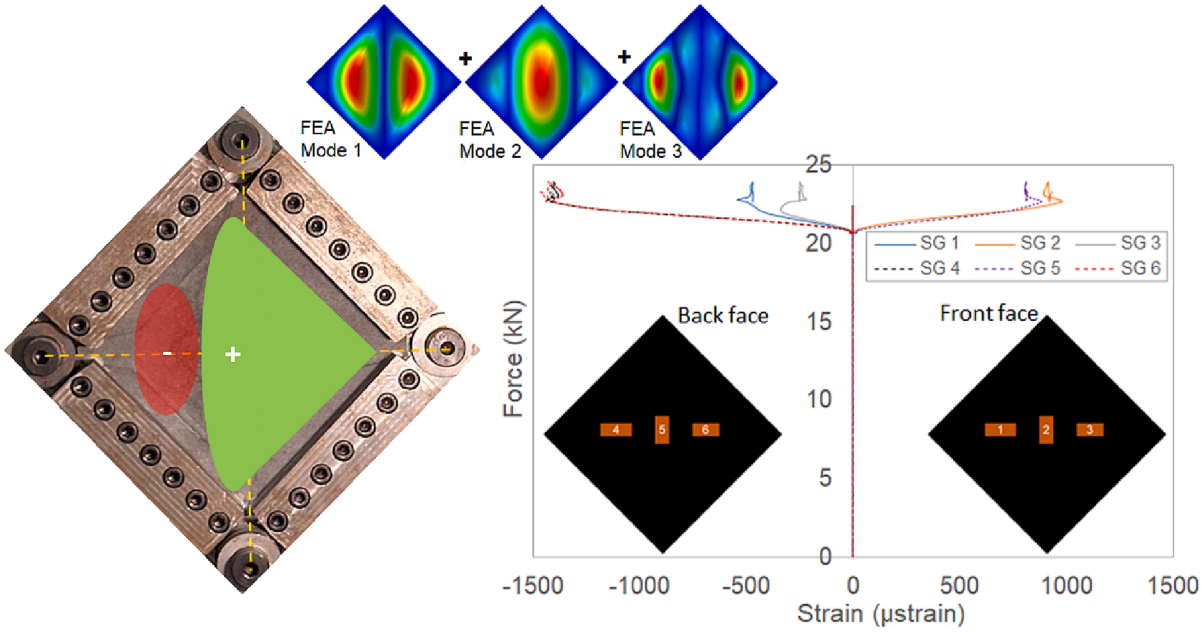

Fig. 24. Experimental buckling mode shape and strain gauge readings.

Declaration of Competing Interest

The authors declare that they have no known competing financial interests or personal relationships that could have appeared to influence the work reported in this paper.

Acknowledgements

The authors express their gratitude to Douglas Nash, Mark Allonby and Daniel Cole (technicians at UWE) for their assistance and facilitating the research.

References

[1] Damghani M, Ersoy N, Piorkowski M, Murphy A. Experimental evaluation of residual tensile strength of hybrid composite aerospace materials after low velocity impact. Compos B Eng 2019;179:107537.
[2] Hozić D, Thore CJ, Cameron C, Loukil M. A new method for simultaneous material and topology optimization of composite laminate structures using Hyperbolic Function Parametrization. Compos Struct Nov. 2021;276:114374. https://doi.org/10.1016/J.COMPSTRUCT.2021.114374.
[3] J. C. Martin, "Composite Optimisation Techniques for Aircraft Components Structural Sizing," in *8th EUROPEAN CONFERENCE FOR AERONAUTICS AND SPACE SCEINCES (EUCASS)*, 2019. doi: 10.13009/EUCASS2019-268.
[4] Ghiasi H, Pasini D, Lessard L. Optimum stacking sequence design of composite materials Part I: Constant stiffness design. Compos Struct Sep. 2009;90(1):1–11. https://doi.org/10.1016/J.COMPSTRUCT.2009.01.006.
[5] Setoodeh S, Abdalla MM, Gürdal Z. Design of variable–stiffness laminates using lamination parameters. Compos B Eng Jun. 2006;37(4–5):301–9. https://doi.org/10.1016/J.COMPOSITESB.2005.12.001.
[6] Xu Y, Zhu J, Wu Z, Cao Y, Zhao Y, Zhang W. A review on the design of laminated composite structures: constant and variable stiffness design and topology optimization. Adv Compos Hybrid Mater 2018;1(3):460–77. https://doi.org/10.1007/s42114-018-0032-7.
[7] Ding H, Xu B. A novel discrete–continuous material orientation optimization model for stiffness-based concurrent design of fiber composite. Compos Struct Oct. 2021;273:114288. https://doi.org/10.1016/J.COMPSTRUCT.2021.114288.
[8] Guimarães TAM, Castro SGP, Cesnik CES, Rade DA. Supersonic Flutter and Buckling Optimization of Tow-Steered Composite Plates. AIAA J Dec. 2018;57(1):397–407. https://doi.org/10.2514/1.J057282.
[9] Nishi S, Terada K, Kato J, Nishiwaki S, Izui K. Two-scale topology optimization for composite plates with in-plane periodicity. Int J Numer Meth Eng Feb. 2018;113(8):1164–88. https://doi.org/10.1002/nme.5545.
[10] Kaveh A, Dadras A, Geran Malek N. Optimum stacking sequence design of composite laminates for maximum buckling load capacity using parameter-less optimization algorithms. Eng Comput 2019;35(3):813–32. https://doi.org/10.1007/s00366-018-0634-2.
[11] J. B. Bai *et al.*, "Determining the best practice – Optimal designs of composite helical structures using Genetic Algorithms," *Compos Struct*, vol. 268, p. 113982, Jul. 2021, doi: 10.1016/J.COMPSTRUCT.2021.113982.
[12] Alcántar V, Aceves SM, Ledesma E, Ledesma S, Aguilera E. Optimization of Type 4 composite pressure vessels using genetic algorithms and simulated annealing. Int J Hydrogen Energy Jun. 2017;42(24):15770–81. https://doi.org/10.1016/J.IJHYDENE.2017.03.032.
[13] Tao W, Liu Z, Zhu P, Zhu C, Chen W. Multi-scale design of three dimensional woven composite automobile fender using modified particle swarm optimization algorithm. Compos Struct Dec. 2017;181:73–83. https://doi.org/10.1016/J.COMPSTRUCT.2017.08.065.
[14] Wang W, Guo S, Chang N, Yang W. Optimum buckling design of composite stiffened panels using ant colony algorithm. Compos Struct Feb. 2010;92(3):712–9. https://doi.org/10.1016/J.COMPSTRUCT.2009.09.018.
[15] Herencia JE, Haftka RT, Weaver PM, Friswell MI. Lay-Up Optimization of Composite Stiffened Panels Using Linear Approximations in Lamination Space. AIAA J Sep. 2008;46(9):2387–91. https://doi.org/10.2514/1.36189.
[16] Zhang J, Zhang W-H, Zhu J-H. An extended stress-based method for orientation angle optimization of laminated composite structures. Acta Mech Sin 2011;27(6):977–85. https://doi.org/10.1007/s10409-011-0506-0.
[17] Ghashochi Bargh H, Sadr MH. Stacking sequence optimization of composite plates for maximum fundamental frequency using particle swarm optimization algorithm. Meccanica 2012;47(3):719–30. https://doi.org/10.1007/s11012-011-9482-5.
[18] Koide RM, Franca GVZ, Luersen MA. An ant colony algorithm to lay-up optimisation of laminated composite plates. Latin American J Solids Struct 2013;10(3):491–504. https://doi.org/10.1590/S1679-78252013000300003.
[19] Farsadi T, Rahmanian M, Kurtaran H. Nonlinear lay-up optimization of variable stiffness composite skew and taper cylindrical panels in free vibration. Compos Struct Apr. 2021;262:113629. https://doi.org/10.1016/J.COMPSTRUCT.2021.113629.
[20] Macquart T, Maes V, Bordogna MT, Pirrera A, Weaver PM. Optimisation of composite structures – Enforcing the feasibility of lamination parameter constraints with computationally-efficient maps. Compos Struct May 2018;192:605–15. https://doi.org/10.1016/J.COMPSTRUCT.2018.03.049.
[21] Bohrer RZG, Kim IY. Concurrent topology and stacking sequence optimization of composite laminate plates using lamination parameters. Compos Struct Nov. 2021;276:114556. https://doi.org/10.1016/J.COMPSTRUCT.2021.114556.
[22] Liu X, Featherston CA, Kennedy D. Buckling optimization of blended composite structures using lamination parameters. Thin-Walled Struct Sep. 2020;154:106861. https://doi.org/10.1016/J.TWS.2020.106861.
[23] Damghani M, Wallis C, Bakunowicz J, Murphy A. Using laminate hybridisation (CFRP-GFRP) and shaped CFRP plies to increase plate post-buckling strain to failure under shear loading. Thin-Walled Struct 2021;162:107543. https://doi.org/10.1016/j.tws.2021.107543.
[24] Damghani M, Pir RA, Murphy A, Fotouhi M. Experimental and numerical study of hybrid (CFRP-GFRP) composite laminates containing circular cut-outs under shear loading. Thin-Walled Struct 2022;179:109752. https://doi.org/10.1016/j.tws.2022.109752.
[25] "Optistruct." Altair Engineering, Inc., Troy MI, United States. [Online]. Available: https://altairhyperworks.com/product/HyperMesh.
[26] Vu-Huu T, Le-Thanh C, Nguyen-Xuan H, Abdel Wahab M. "Incompressible Fluid Computation Based on Polygonal Finite Element BT -. In: Proceedings of the 1st

International Conference on Numerical Modelling in Engineering"; 2019. p. 202–12.
[27] Nakshatrala KB, Masud A, Hjelmstad KD. On finite element formulations for nearly incompressible linear elasticity. Comput Mech 2008;41(4):547–61. https://doi.org/10.1007/s00466-007-0212-8.
[28] K.-H. Chang, "Chapter 4 - Structural Design Sensitivity Analysis," Elsevier Inc, 2015, pp. 211–323. doi: 10.1016/B978-0-12-398512-5.00004-9.
[29] Damghani M, Saddler J, Sammon E, Atkinson GA, Matthews J, Murphy A. An experimental investigation of the impact response and Post-impact shear buckling behaviour of hybrid composite laminates. Compos Struct 2023;305:116506. https://doi.org/10.1016/j.compstruct.2022.116506.
[30] Her S-C. Stress analysis of ply drop-off in composite structures. Compos Struct 2002;57(1):235–44. https://doi.org/10.1016/S0263-8223(02)00090-9.
[31] Mukherjee A, Varughese B. Design guidelines for ply drop-off in laminated composite structures. Compos B Eng 2001;32(2):153–64. https://doi.org/10.1016/S1359-8368(00)00038-X.
[32] Shim D-J, Lagace PA. Mechanisms and Structural Parameters Affecting the Interlaminar Stress Field in Laminates with Ply Drop-offs. J Compos Mater Jul. 2005;40(4):345–69. https://doi.org/10.1177/0021998305055192.
[33] Torres M, Collombet F, Douchin B, Crouzeix L, Grunevald Y-H. Numerical and experimental value added of Multi-Instrumented Technological Evaluator for the analysis of thick monolithic composite structures with singularity details. Compos Struct 2015;127:41–50. https://doi.org/10.1016/j.compstruct.2015.02.075.